European Journal of Medicinal Chemistry 302 (2026) 118338

Contents lists available at ScienceDirect

European Journal of Medicinal Chemistry

journal homepage: www.elsevier.com/locate/ejmech

Research paper

An adamantylureido-benzylamide aniline as FLAP/sEH dual inhibitor: Rational design, *in vitro* and *in vivo* lipidomic profiling

Tania Ciaglia [a,1], Danilo D'Avino [b,1], Paul M. Jordan [c,1], Simone Di Micco [d], Simona Musella [a], Hannes Engelbrecht [c], Lukas Klaus Peltner [c], Veronica Di Sarno [a], Fabrizio Merciai [a], Sara Perna [b], Gerardina Smaldone [a], Francesca Di Matteo [a], Valeria Napolitano [a], Rosario Stimoli [a,e], Giuseppe Bifulco [a], Giacomo Pepe [a], Eduardo Maria Sommella [a], Manuela Giovanna Basilicata [f], Giovanna Aquino [a,g], Isabel M. Gomez-Monterrey [b], Pietro Campiglia [a], Carmine Ostacolo [a], Oliver Werz [c], Antonietta Rossi [b,*], Alessia Bertamino [a,**], Michele Manfra [h]

[a] Department of Pharmacy, University of Salerno, Via G. Paolo II 132, Fisciano, Salerno, Italy, 84084
[b] Department of Pharmacy, School of Medicine and Surgery, University of Naples Federico II, Via D. Montesano 49, 80131, Naples, Italy
[c] Department of Pharmaceutical/Medicinal Chemistry, Institute of Pharmacy, Friedrich Schiller University, Philosophenweg 14, D-07743, Jena, Germany
[d] European Biomedical Research Institute of Salerno (EBRIS), Via S. De Renzi 50, 84125, Salerno, Italy
[e] National PhD Program in "RNA Therapeutics and Gene Therapy", Napoli, Italy
[f] Department of Advanced Medical and Surgical Sciences, University of Campania "Luigi Vanvitelli", P.zza L. Miraglia, 2, 80138, Naples, Italy
[g] AREA Science Park, Laboratorio di Multi-omica Area Sud (LAAS), Baronissi, Salerno, 84081, Italy
[h] Department of Science, University of Basilicata, Via Dell'Ateneo Lucano 10, Potenza, 85100, Italy

A B S T R A C T

Multitarget approaches are highly effective strategies for treating acute and chronic inflammatory diseases. In this field, the dual inhibition of 5-lipoxygenase-activating protein (FLAP) and soluble epoxide hydrolase (sEH) offers the advantage of reducing the production of diverse pro-inflammatory lipid mediators (LMs) while preserving pro-resolving mediator levels. However, this approach is underexplored in medicinal chemistry, given the limited number of existing dual inhibitors. Here, we present the rational design of the adamantylureido-benzylamide aniline **6**, which features *in vitro* FLAP/sEH inhibitory activity. An accurate investigation about the crucial interactions between our synthesized derivatives and 5LOX, FLAP and sEH binding sites, led us to shed light on structural requirements differentiating among the three targets. Lipidomic profiling following **6** *in vivo* administration highlighted the reduction of 5-LOX/FLAP- and sEH-derived LMs, resulting in a favourable redistribution of LMs in agreement with the inhibition of its molecular targets.

1. Introduction

Inflammation is a host response to various noxious stimuli, including thermal, mechanical, chemical injuries, as well as pathogenic infections. The primary goal of the inflammatory response is to remove harmful stimuli and promote the healing process, thereby restoring the organism's homeostasis. If resolution of inflammation fails, the process can become chronic, contributing to a broad spectrum of chronic inflammatory diseases such as asthma, heart disease, cancer, obesity, and many others [1]. The inflammatory response is tightly regulated by lipid mediators (LMs) such as prostanoids, leukotrienes (LTs), epoxyeicosatrienoic acids (EETs), and specialized pro-resolving mediators (SPMs), whose biosynthesis starts with the release of polyunsaturated fatty acids (PUFAs) from membrane phospholipids. In particular, free arachidonic acid (AA) serves as substrate for three enzymatic branches: cyclooxygenase (COX), lipoxygenase (LOX), and cytochrome P450 (CYP450) pathways, each generating a broad range of LMs [2]. All these metabolites have been intensely investigated for their crucial role in orchestrating the propagation and the resolution of the inflammatory cascade. Prostanoids are produced by the activity of COXs, and primarily play a pro-inflammatory role. However, some prostanoids, such as PGE_2 and PGD_2, can exert an anti-inflammatory

* Corresponding author.
** Corresponding author.
E-mail addresses: antrossi@unina.it (A. Rossi), abertamino@unisa.it (A. Bertamino).
[1] These authors contributed equally to this work.

https://doi.org/10.1016/j.ejmech.2025.118338
Received 25 September 2025; Received in revised form 23 October 2025; Accepted 2 November 2025
Available online 3 November 2025

actions depending on the context and the cellular target [3].

Pro-inflammatory LTs derive from the 5-LOX pathway, involving the 5-LOX-activating protein (FLAP) that is devoid of enzymatic activity and assists 5-LOX in the initial steps of LT biosynthesis, providing AA as substrate [4,5]. 5-LOX also metabolizes other PUFAs such as eicosapentaenoic acid (EPA) and docosahexaenoic acid (DHA) into bioactive LMs, which contribute to resolving inflammation [6]. However, the involvement of FLAP in SPM biosynthesis via 5-LOX depends on the PUFA, where EPA and AA but not DHA are utilized by FLAP as 5-LOX substrates for SPM production [7,8].

EETs derive from AA after conversion by CYP450, and their role as endogenous anti-inflammatory LMs has been well characterized. Nevertheless, upon formation, EETs survive only for a very short time in the bloodstream due to their hydrolysis and inactivation by soluble epoxide hydrolase (sEH), which converts them into the corresponding pro-inflammatory dihydroxyeicosatrienoic acid (DiHET) derivatives [9]. EETs possess anti-inflammatory, analgesic, anti-migratory, and fibrinolytic properties, and their pathway modulation represents a fruitful therapeutic option in the anti-inflammatory field [10,11]. In this regard, inhibition of sEH leads to an increased concentration of EETs and a concomitant reduction in the production of pro-inflammatory DiHETs, thereby attenuating inflammation in experimental models of acute and chronic inflammation [12,13].

To date, nonsteroidal anti-inflammatory drugs (NSAIDs), which inhibit prostanoid biosynthesis, represent the pillar of the anti-inflammatory treatment; however, they are plagued by several and serious side effects, especially at cardiovascular and gastrointestinal levels [14–16]. Current developments in the design of new anti-inflammatory compounds are oriented toward multitarget approaches, intended to facilitate simultaneous interaction with two or more enzymes involved in the formation and degradation of LMs. This path is particularly pursued because it enables the enhancement of efficacy and safety in the treatment of inflammation-related disorders [17–19].

Recently, we conducted a drug discovery campaign with the aim of identifying novel anti-inflammatory compounds that act via alternative mechanisms than those of NSAIDs. We developed a dual 5-LOX/sEH inhibitor (compound **73**, Fig. 1), which has been validated using *in vivo* murine models of inflammation [20]. Moving forward this research and exploiting the previously acquired information, we obtained a selective sEH inhibitor (compound **28**, Fig. 1), with *in vivo* anti-inflammatory activities [21]. Taking advantage of our previous findings in this field, here we report the identification of a dual FLAP/sEH inhibitor (compound **6**, Fig. 1), obtained through *in-silico* design. Derivative **6** was validated by *in vitro* testing its inhibitory activity on human isolated sEH, verifying the lack of activity against 5-LOX, and assessing its activity in human neutrophils in the absence or presence of exogenous AA. Thus, we investigated about compound **6** selectivity, observing no activity against COXs and mPGES1 and finally we continued with its *in vivo* pharmacological characterization, profiling the mice lipidome after derivative **6** administration.

We shifted our interests toward FLAP instead of 5-LOX, considering the aim of inhibiting pro-inflammatory LT production, while preserving SPM formation from DHA. At the same time, sEH inhibition allows the increase of EET levels, exploiting their anti-inflammatory properties [22–26]. This pharmacological strategy has been well validated, as demonstrated by the number of sEH inhibitors subjected to clinical trials [27–29]. In contrast, despite several FLAP inhibitors disclosed so far, none of them have reached the pharmaceutical market, principally because of their poor pharmacokinetic [30,31]. Contextually, FLAP/sEH dual inhibition remains a largely unexplored area, with diflapolin and its derivatives (Fig. 1) currently the only known compounds exhibiting this profile [32,33].

2. Results and discussion

2.1. Chemistry

Final derivatives **1–6** were synthesized in accordance with Scheme 1. 2, 4-Dinitrobenzoic acid was first converted into the corresponding methyl ester intermediate **a** (98 % yield) by microwave irradiation in acid medium and then reduced to the phenylenediamine-based compound **b** in presence of ammonium formate and Pd/C as catalyst, in almost quantitive yield. The subsequent reaction with cyclohexylamine

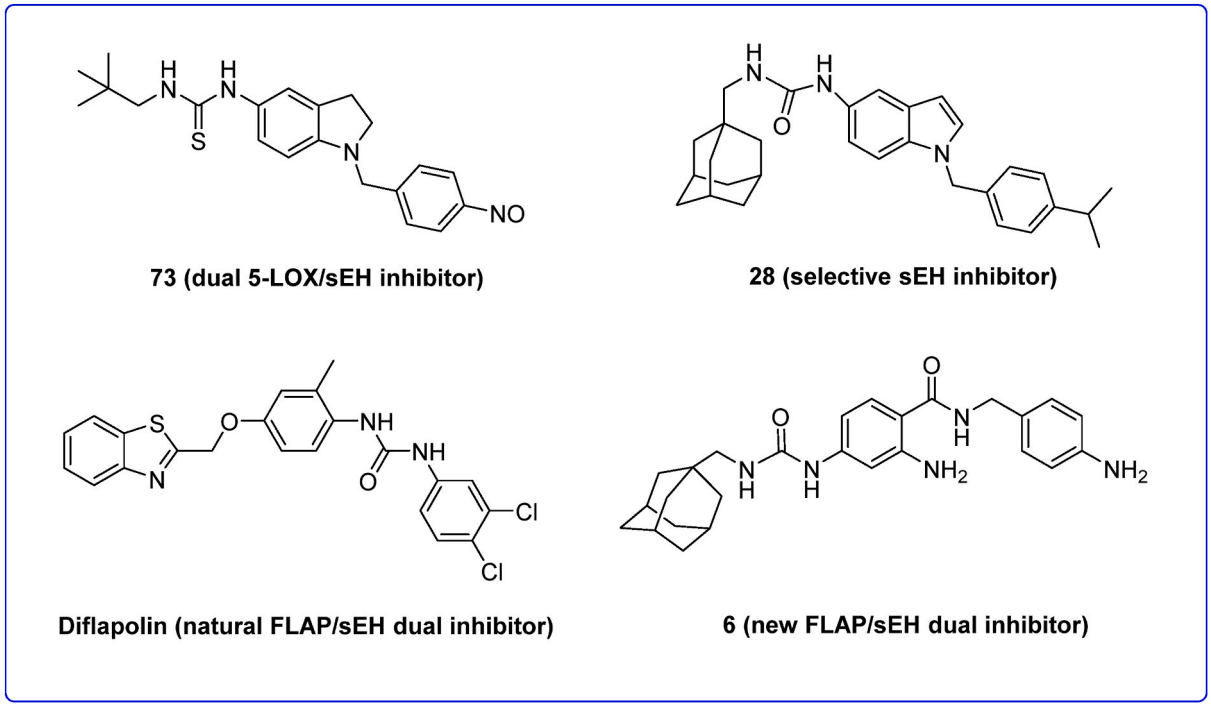

Fig. 1. Chemical structure of previously synthesized compounds **73** and **28**, diflapolin and the new FLAP/sEH inhibitor **6**.

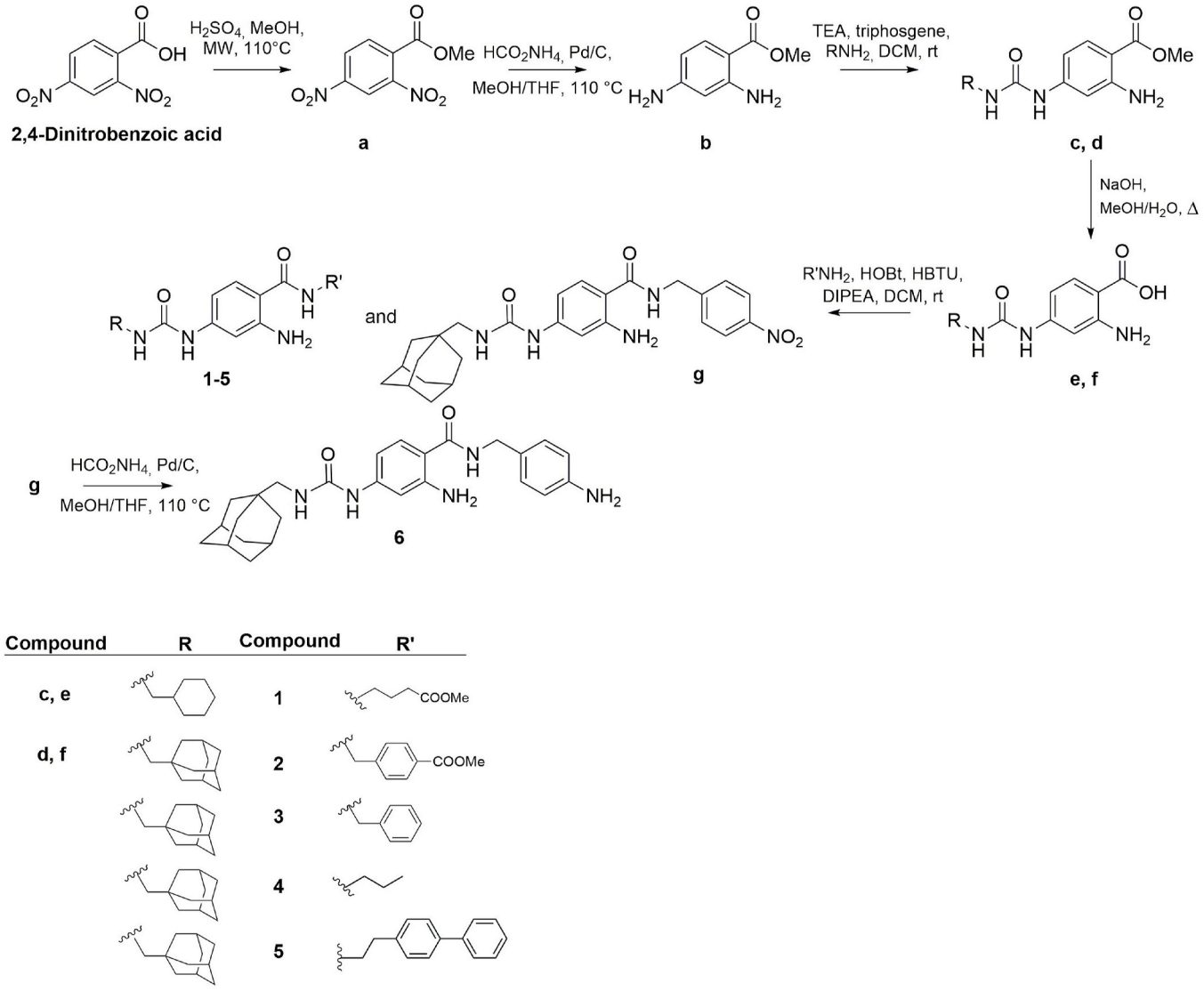

Scheme 1. Synthesis of the derivatives **1–6**.

or 1-adamantanmethylamine using triethylamine as base and triphosgene as carbonyl group donor led to the urea intermediates **c** and **d** (43 and 53 % yield). After basic hydrolysis the corresponding carboxylic acid **e** and **f** were coupled with methyl 4-aminobutyrrate, methyl 4-aminomethyl benzoate, benzylamine, 1-propylamine, 2-(4-biphenyl) ethylamine or 4-nitrobenzylamine yielding, respectively, final compounds **1–5** and intermediate **g** in 52–66 % of yield. Intermediate **g** was further reduced under the conditions described above, giving the final derivative **6** (55 % yield).

Compounds **7–14** were obtained applying the synthetic procedures depicted in Scheme 2. For the synthesis of **7** and **8** 2-nitro-1,4-phenylenediamine was reacted with methyl 4-formylbenzoate under reductive amination conditions, furnishing intermediate **h** in 75 % of yield. Then, reaction with benzyl chloroformate in basic medium led to the amino-protected compound **i** (92 % yield), which has been converted into the urea **j** by reaction with 1-adamantanmethylamine in the previously reported conditions (56 % yield). The following reduction of the nitro group quantitatively gave the compound **7**, which was further hydrolysed in basic medium, furnishing the corresponding carboxylic derivative **8** in 92 % of yield.

Final derivatives **9** and **10** were obtained using 1,4-phenylenediamine as starting material. It was first converted into the urea intermediate **k** (44 % yield), by reaction with 1-adamantanmethylamine, and then alkylated with methyl 4-(bromomethyl)benzoate or 4-nitrobenzyl chloride using potassium *tert*-butoxide as base under microwaves irradiation, yielding final compound **9** (54 % yield) and intermediate **l** (46 % yield). The latter was further reduced under the above described conditions furnishing the amino-derivative **10** (51 % yield).

2-Methoxy-4-nitroaniline was employed for the synthesis of **11**–**14**. The starting material was protected using di-*tert*-butyl dicarbonate as Boc group donor and DIPEA as base leading to the intermediate **m** (78 % yield), which was reduced at the position 4, and converted into the urea intermediates **o** and **p** (44–51 % yield). The acid-based Boc deprotection, using TIS as scavenger, and the following alkylation with methyl 4-(bromomethyl)benzoate or 4-nitrobenzyl chloride led to the final compound **11** and to intermediates **q** and **r** (45–50 % yield). Derivative **11** and intermediate **q** were hydrolysed to the corresponding carboxylic acids **12** and **13** in almost quantitative yield, while **r** was reduced to the final amino compound **14** as described above (92 % yield)

Derivatives **15** and **16** were synthetized as depicted in Scheme 3. 4-Nitrophenol reacted with methyl 4-(bromomethyl)benzoate in the conditions described above leading to the alkylated intermediate **s** (71 % yield). Then, it was subjected to the reduction of the nitro group at position 4 (**t**, 98 % yield) and, further derivatized to the ureidic compound **u** in presence of 1-adamantanmethylamine (46 % yield). The final basic hydrolysis led to **15** in almost quantitative yield. For the synthesis

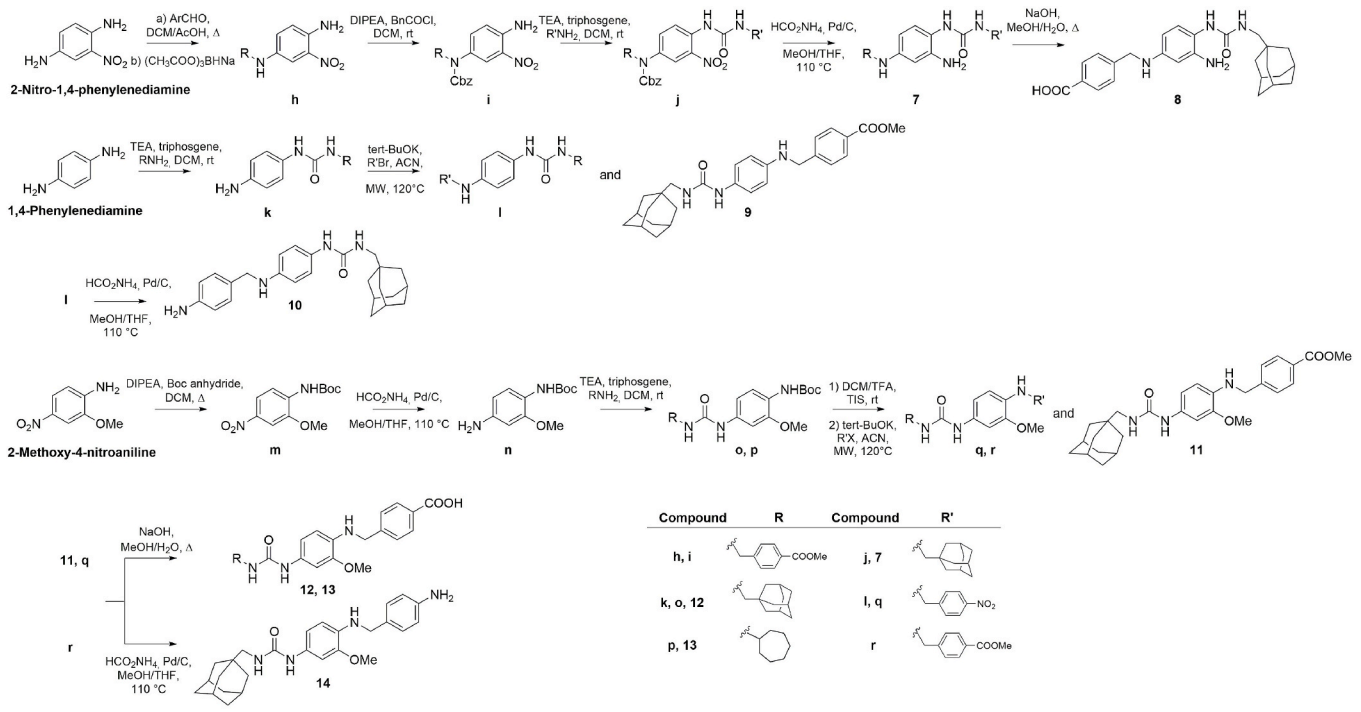

Scheme 2. Synthesis of the derivatives **7–14**.

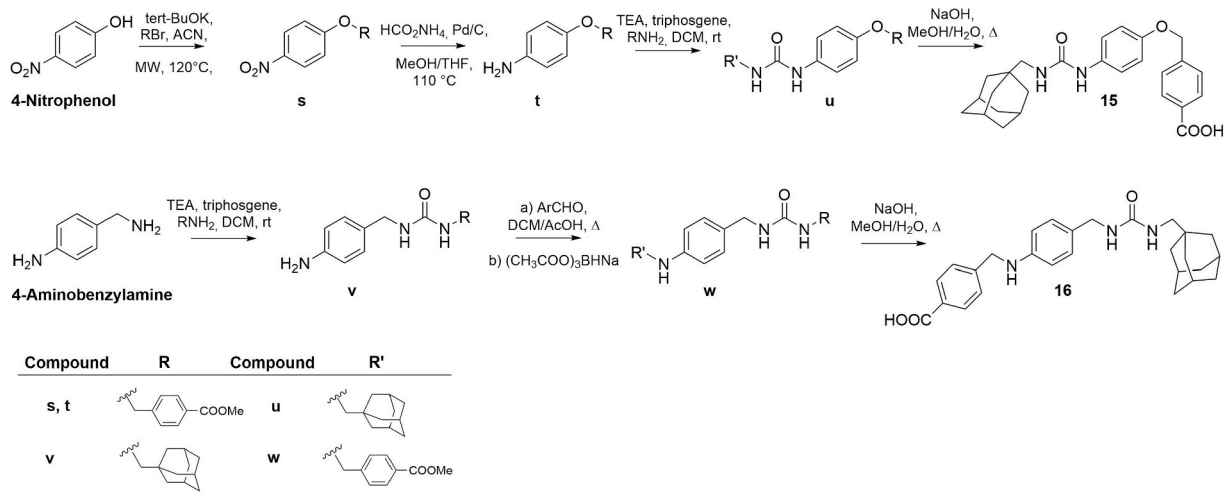

Scheme 3. Synthesis of the derivatives **15** and **16**.

of **16**, 4-aminobenzylamine, employed as starting material, was first converted into the urea **v** (45 % yield), alkylated by reductive amination in presence of methyl 4-formyl benzoate and finally hydrolysed furnishing derivative **16** (92 % yield), applying the reaction conditions previously reported.

2.2. Molecular docking and biological evaluation

In our recent contribution on indoline-based dual inhibitors against 5-LOX and sEH, we demonstrated that the 1-(adamantan-1-ylmethyl)-urea group, bound to an aromatic ring, is fundamental for sEH inhibition [21]. These structural features were merged with the reported observations that different known inhibitors of FLAP present a conserved central phenyl substructure properly substituted [34–36]. Thus, we designed a new small library of 16 tri-substituted aryl-derivatives as potential sEH/FLAP inhibitors. Firstly, the designed molecules were synthesized and then assessed *in vitro* to evaluate their inhibitory activity against sEH and 5-LOX/FLAP.

The *in vitro* tests against isolated sEH enzyme highlighted that most compounds are active in nanomolar range with diverse efficiencies. Five out of the 16 small molecules, namely **6**, **9**, **10**, **11**, and **12**, showed very potent inhibition ($IC_{50} < 13$ nM, Table 1). These compounds fit well into the binding site in equivalent spaces and share the same network of intermolecular interactions through their common structural moieties (Fig. 2A–D,4A). Specifically, the urea donates two H-bonds to D335 and accepts two ones from Y383 and Y466. The adamantyl moiety gives van der Waals contacts with Y336, M339, T360, F381, Q384, L499, M503. The phenyl ring linked to urea group establishes π-π interaction with H524 (Fig. 2A–D,4A). Noteworthy, these described ligand-protein interactions are also observable for the compound 34 N, which was co-crystallized with sEH [37]. The urea also establishes two aromatic H-bonds with Y383 and Y466. Moreover, the central phenyl group of **9**

Table 1
Inhibition of human isolated sEH and human isolated 5-LOX. All values are given as mean ± SEM of single determinations obtained in 3–4 independent experiments.

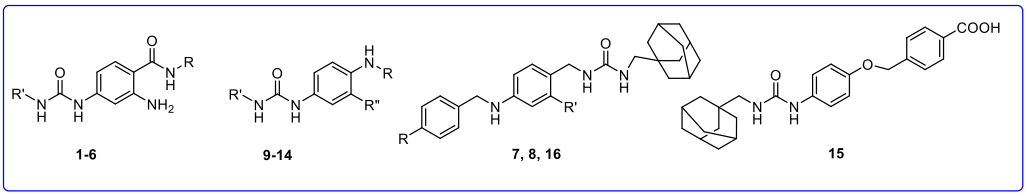

Compound	R	R_1	R"	IC_{50} for sEH (nM)	IC_{50} for 5-LOX (μM)
1	COOMe–$(CH_2)_3$–	CyclohexylCH_2-	–	4029.7 ± 1298.4	ND
2	4-COOMe-PhCH_2-	AdamantylCH_2-	–	502.2 ± 255.2	ND
3	PhCH_2-	AdamantylCH_2-	–	>10,000	>10
4	$(CH_2)_2$ CH_3-	AdamantylCH_2-	–	>10,000	>10
5	4-Ph-Ph$(CH_2)_2$-	AdamantylCH_2-	–	>10,000	>10
6	**4-NH_2-PhCH_2-**	**AdamantylCH_2-**	**-**	**12.6 ± 3.5**	**> 10**
7	COOMe-	NH_2	–	21.8 ± 2.2	0.56 ± 0.34
8	COOH	NH_2	–	56.3 ± 16.8	3.40 ± 1.09
9	4-COOMe-PhCH_2-	AdamantylCH_2-	H	2.6 ± 0.9	0.39 ± 0.12
10	4-NH_2-PhCH_2-	AdamantylCH_2-	H	1.7 ± 0.4	0.86 ± 0.27
11	4-COOMe-PhCH_2-	AdamantylCH_2-	OCH_3	2.8 ± 1.5	0.50 ± 0.25
12	4-COOH-PhCH_2-	AdamantylCH_2-	OCH_3	8.9 ± 3.2	3.21 ± 1.29
13	4-COOH-PhCH_2-	CycloheptanylCH_2-	OCH_3	525.9 ± 88.5	7.04 ± 2.70
14	4-NH_2-PhCH_2-	AdamantylCH_2-	OCH_3	72.2 ± 12.5	0.40 ± 0.20
15	–	–	–	37.0 ± 0.8	>10
16	COOH	H	–	20.7 ± 3.9	ND

ND = not determined.

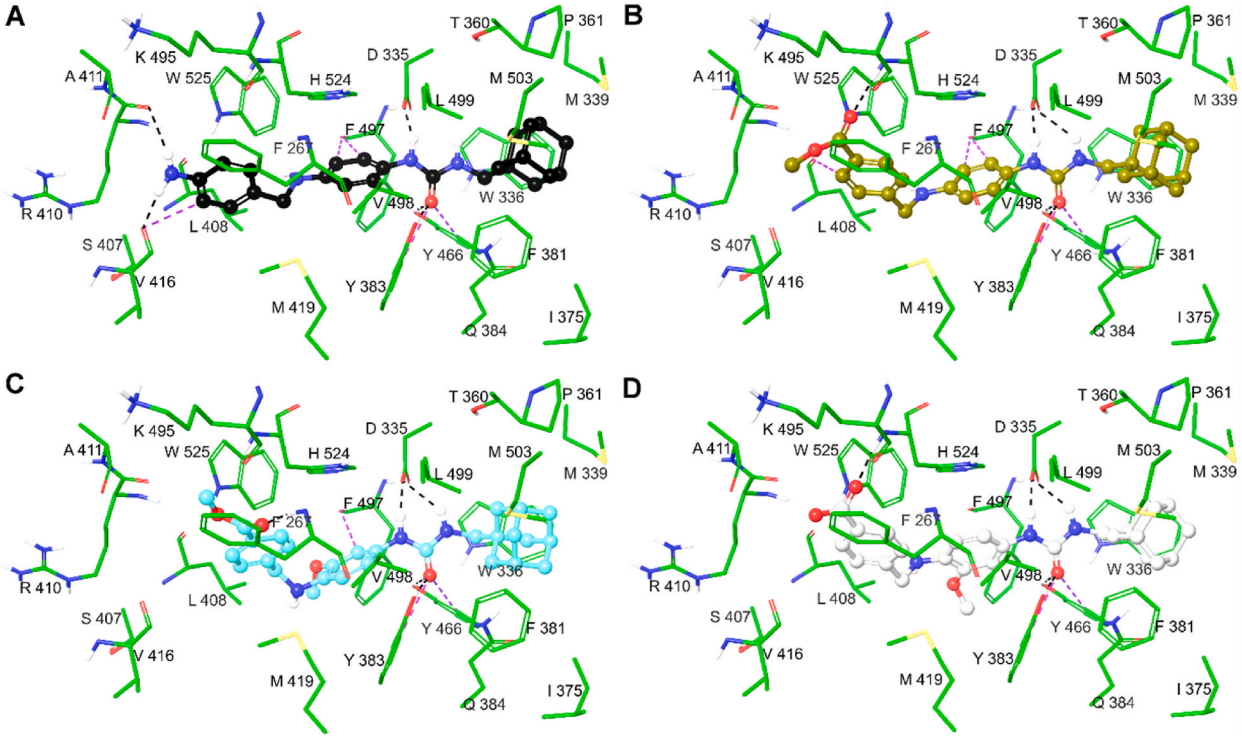

Fig. 2. Three-dimensional model of the interactions given by **10** (A), **9** (B), **11** (C) and **12** (D) with sEH. The protein is depicted by green tube with the atom colour code: C, green; polar H, white; N, dark blue; O, red; S, yellow). The small molecules are represented by sticks (black for **10**, kiwi for **9**, cyan for **11**, light grey for **12**) and balls (with the atom colour code used for the protein except for C, as for the sticks). The dashed black and violet lines indicate respectively the hydrogen bond and aromatic H-bond between the ligand and protein.

and **10** gives two aromatic H-bonds with the backbone CO of F267, while **11** only one. The methoxy group of **11** accepts an aromatic H-bond from the side chain of F267. Instead, **6** is hydrogen-bonded to the F267 CO by the amino group on the central phenyl ring (Fig. 4A). Compound **12** does not show these aromatic H-bonds, justifying a slightly higher IC_{50} than **9**, **10** and **11**. The benzyl group of **9**, **10**, **11**, gives π-π interaction with W525. The same cyclic moiety of **10** establishes also an aromatic-bond and two hydrogen bonds by its amino group at C-4 with backbone CO of R410 and V416 (Fig. 2A). The ester group of **9** and **11** accepts a H-bond from the NH backbone of H524 and F497, respectively.

The carboxylic acid of **12** gives the same interaction of the ester group of **9**. Compound **6** structurally differs from **9**, **10**, **11** and **12** for an amide linker between the two aromatic rings instead of an amine. Despite an aromatic H-bond of the aniline moiety, respectively, with backbone CO of R410 and K495, the higher linker length of **6** increases the distance from W525, lowering the strength of the π stacking, in agreement with the obtained IC_{50} of 19 nM. The compounds **7**, **8**, **14**, **15**, and **16** presented a lower inhibitory profile, varying from 20 nM to 73 nM (Table 1), than the congeners above described. The amine at C-2 of central phenyl of **7** and **8** is not involved in hydrogen bond and impedes the π stacking with H524 (Fig. S49A and B). Even though the amine at C-4 of benzyl of **14** is H-bonded to side chain of S415, no π stacking with H525 is established (Fig. S49C). Moreover, the presence of a methoxy group disfavours the formation of aromatic H-bonds by the central aromatic cycle. The oxygen linker of **15** is engaged in an aromatic H-bond with W525 displacing and 90° rotating the central phenyl from H524 with the loss of π-π interaction (Fig. S49D). Differently from its analogues, **16** is endowed with a methylene between the urea and central aromatic ring, inducing a 90° rotation of the phenyl respect to **6**, **9**, **10**, **11**, and **12** (Fig. S49E). This rotation causes the loss of the aromatic H-bond and lowers the strength of π stacking with H524 by incrementing the distance between the planar counterparts, raising its IC_{50} respect to **6**, **9**, **10**, **11**, and **12**. As **6**, **2** has a methyl amide linker between the two aromatic rings but with an ester group instead of an amine at C-4 of benzyl (Fig. S50A). The presence of the bulkier ester group induces the loss of a hydrogen bond by urea and by the amine at C-2 of the phenyl ring, reducing the inhibitory activity (**2** IC_{50} = 502.2 *vs* **6** IC_{50} = 12.6 nM). Compounds **1** and **13** replace the adamantly group respectively with a cyclohexyl and cycloheptyl (Fig. S50B and C). According to our previous studies [21], the adamantly replacement lowers, also for this scaffold, the van der Waals contacts with the surrounding residues, giving rise to poorer inhibitor activity. Moreover, **7** also presents a carbon chain instead of a benzyl group losing the π stacking with W525, leading to an around eight times higher IC_{50} than **13.** In agreement with experimental values, no optimal interactions with sEH binding cavity and not plausible docked poses were found for **3–5**.

Next, to evaluate the bioactivity of the synthetized compounds against 5-LOX and FLAP, we employed well-established cell-free (FLAP-independent) and cell-based (FLAP-dependent) test systems [38]. The cell-free assay utilizes isolated human recombinant 5-LOX, with 20 μM AA provided as a substrate for enzymatic conversion in the absence of FLAP. For the analysis of 5-LOX and/or FLAP inhibition in intact cells (cell-based assay), we used human neutrophils stimulated with the calcium ionophore A23187. In this setup, the exogenous addition of AA (20 μM) at least partially bypasses the requirement for FLAP in LT formation (Table 2). The *in vitro* tests with isolated 5-LOX revealed inhibitory activity only for compounds endowed with methylamine linker between the aromatic rings and the urea directly bound to the phenyl (**7–14**; 0.39 ± 0.12 μM ≤ IC_{50} ≤ 7.04 ± 2.70 μM, Table 1). Conversely, scarce/absent inhibition of 5-LOX is observed for the other analogues. Theoretical studies suggested that the methylamine moiety is H-bonded to the Fe^{2+} coordinating residue I673, allowing the correct accommodation of side aromatic ring to form a π-cation with catalytic ion. On the contrary, the replacement of NH with the carbonyl of the amide group induces the loss of this hydrogen bond with I673 and moves away the aromatic portion preventing the occupancy of the open position of Fe^{2+} coordination sphere (Fig. 3). Moreover, we observed that larger molecular size negatively affects the interaction with 5-LOX, causing distorted ligand conformations or no docked poses (Fig. 3).

Considering these preliminary results and taking into account our goal to develop FLAP/sEH inhibitors, we continued our investigation, discarding those derivatives which showed 5-LOX activity (compounds **7–14**), as well as those lacking remarkable sEH inhibition (compounds **1**, **3–5**, **13**). Thus, we selected derivatives **2**, **6**, **15** and **16** for the subsequent evaluation in the cell-based FLAP-dependent system. In this assay, human neutrophils were pretreated by the compounds **2**, **6**, **15** and **16** for 15 min at 10 μM each, and cells were stimulated for 10 min by 2.5 μM of A23187. Then, 5-LOX products (LTB_4, *trans-* and epi-trans-LTB_4 and 5-HETE) were analyzed by RP-HPLC.

As shown in Table 2, only compound **6** was able to suppress 5-LOX product formation by >50 % (residual activity 35.7 %), while compounds **2**, **15** and **16** were poorly active or non-active.

Table 2
Effects of compounds **2**, **6**, **15** and **16** (10 μM) on 5-LOX/FLAP-dependent LM formation in human neutrophils.

Compound	Structure	5-LOX residual activity in neutrophils (%)
2	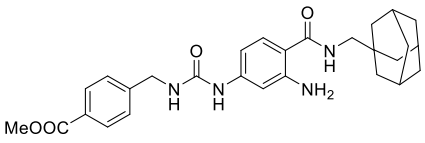	78.8 ± 7.6
6	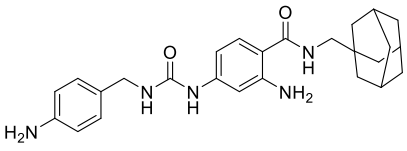	**35.7 ± 5.9**
15	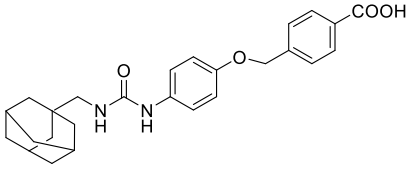	>100
16	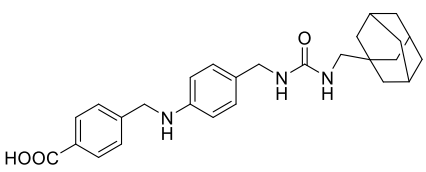	77.5 ± 8.5

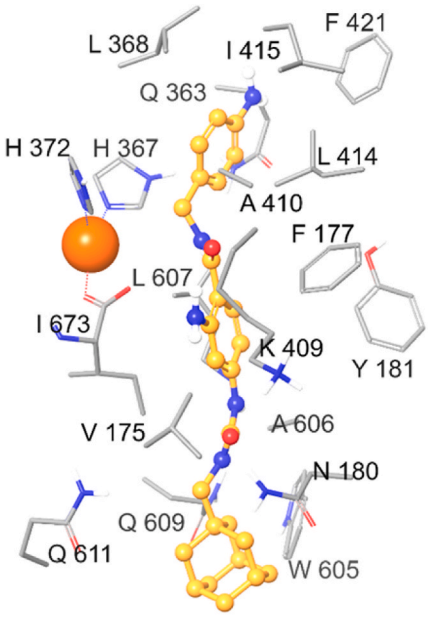

Fig. 3. Three-dimensional model of the interactions given by **6** with 5-LOX. The protein is depicted by grey tube with the atom colour code: C, grey; polar H, white; N, dark blue; O, red. The small molecule is represented by orange sticks and balls (with the atom colour code used for the protein except for C, as for the sticks).

To exclude the requirement of FLAP for 5-LOX product formation in activated PMNL, exogenous AA was added to the incubation media. Of interest, compound **6** lost its potency in the presence of exogenous AA. Thus, in the absence of exogenous AA, the IC_{50} value was determined at 5.4 ± 0.5 μM but when exogenous AA was included in these cell-based assays, the IC_{50} was higher than 10 μM, suggesting that **6** may act via FLAP or, at least, in an AA-competitive manner (Table 3).

To shed light on the peculiar behaviour of **6** and to rationalize its interaction with FLAP, a computational analysis was carried out. Indeed, *in-silico* study suggested that the observed experimental outcomes could be mainly ascribed to the methyl amide linker between two aromatic rings of derivative **6**, which allows a deep penetration into the binding cavity of FLAP with the molecule completely buried into the hydrophobic pocket, placing only the 1-(adamantan-1-ylmethyl)urea near to the protein surface [34–36]. The central phenyl ring of **6** gives van der Waals interactions with chain A residues A63, T66, A113, I119 and G24 of chain C (Fig. 4B). The same interactions are found for benzyl group with residues of chain A A63, T66, and chain C N23, F26, V61, Y64. The benzyl also establishes an aromatic H-bond with the backbone CO of N23 and the side chain of N57 (chain C), while the amide linker is H-bonded to the side chain of T66 of monomer A (Fig. 4B). The amine at C-2 of the central phenyl forms an H-bond with backbone CO of F114 (chain A) and, intriguingly, overlaps the quinoline nitrogen of co-crystallized ligand DG-031 (PDB ID: 6VGC) [34], which engages a water-mediated hydrogen bond with backbone NH of F114A. The other amine group is H-bonded to the side chain of N23 (chain C). The urea group accepts and donates a hydrogen bond respectively to side chain and backbone CO of K116 (chain A). The adamantyl moiety accommodates into an apolar cavity delimited by L120 and F123A of chain A, and V21 oh chain C.

Collectively, in line with our previous contribution to multitargeting drugs [25,26], the structural modifications between the two aromatic rings are crucial to address the macromolecular recognition by small molecules. Indeed, the obtained outcomes suggest that the methyl amide linker led to selective dual FLAP/sEH inhibitors (Fig. 5). The methyl amine switches the binding preference towards both sEH and 5-LOX, moreover, a small linker between 1-(adamantan-1-ylmethyl)urea and

Table 3
IC_{50} values of the lead compound **6** on 5-LOX product formation in human neutrophils in the absence or presence of exogenous AA. Data are means ± S.E.M., n = 3.

	IC_{50} (μM) (w/o AA)	IC_{50} (μM) (+AA)
6	5.4 ± 0.5	>10

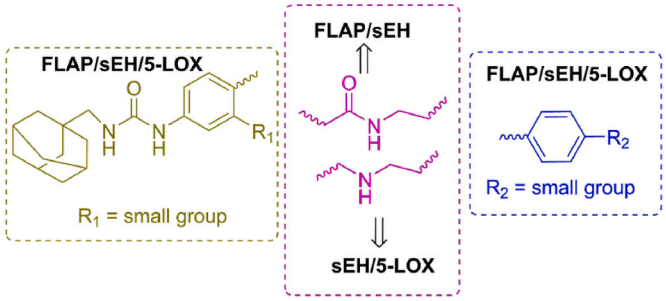

Fig. 5. Schematic representation of the structural modifications carried out to design dual or triple inhibitors.

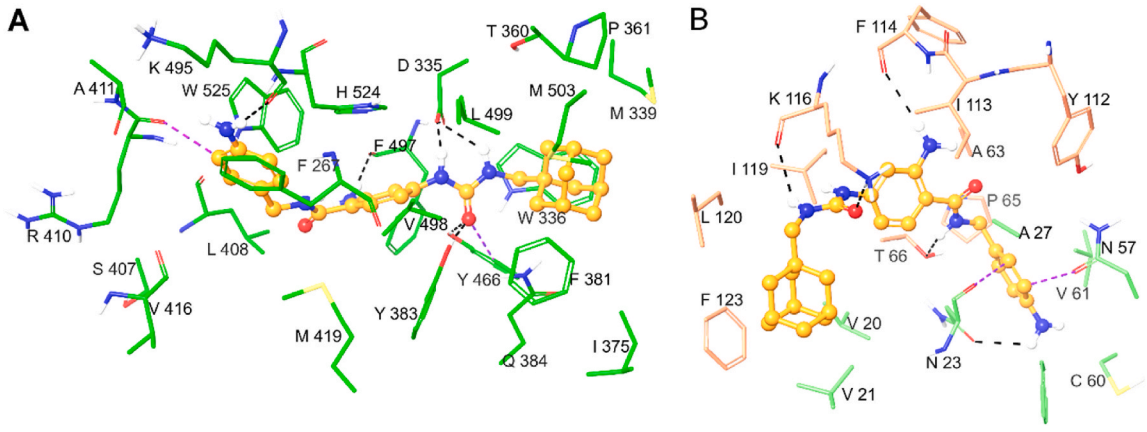

Fig. 4. Three-dimensional model of the interactions given by **6** with sEH (A) and FLAP (B). The protein sEH is represented as in Fig. 2. FLAP is depicted by faded red-orange (chain A) and green (chain C) tube (C, according to chain colour; polar H, white; N, dark-blue; O, red; S, yellow). **6** is represented by orange sticks and balls (with the atom colour code used for the protein except for C, as for the sticks). The dashed black and violet lines indicate respectively the hydrogen bond and aromatic H-bond between the ligand and protein.

central phenyl could be tolerated by sEH. The side molecular moieties of the compounds should appear versatile and could be well tailored to design the aimed inhibitors.

2.3. Compound 6 modulates the lipid mediator class switch in human macrophages

After identifying the dual FLAP/sEH-inhibitory efficiency of compound **6**, we investigated whether compound **6** could inhibit other enzymes within the AA cascade, namely COX-1/2 and mPGES-1. Up to a concentration of 10 μM, compound **6** did not affect the activities of isolated COX-1 (Fig. 6A) and COX-2 (Fig. 6B) or mPGES-1 enriched in microsomes (Fig. 6C) in cell-free assays. Control experiments using the non-selective COX inhibitor indomethacin (indo., 10 μM) and the mPGES-1 inhibitor MK886 (10 μM) confirmed the validity of the assays (Fig. 6A–C). Next, we investigated the capacity of compound **6** to switch the LM profiles in human monocyte-derived macrophages (MDM). We employed pro-inflammatory M1-MDMs and pro-resolving M2-MDM stimulated with exotoxins contained in *Staphylococcus aureus*-conditioned medium (SACM) [39] as test systems. Notably, the M1-MDM subtype abundantly expresses FLAP as well as mPGES-1 and COX-2, and produces high amounts of LTB_4 and PGE_2, while M2-MDM displays lower FLAP, mPGES-1 and COX-2 levels but strongly expresses 15-LOX-1, generating high amounts of 15-LOX products and resolvin D5 (RvD5) upon stimulation with SACM [39]. Compound **6** inhibited the formation of 5-LOX/FLAP-derived LMs in M1-and M2-MDMs, such as LTB_4 and LTC_4, in a concentration-dependent manner, becoming apparent at concentrations as low as 1 μM (Fig. 6D–F). This effect was more pronounced in M1-MDM versus M2-MDM, primarily due to their higher expression of FLAP in M1-MDM, consistent with previous studies [40]. Notably, the formation of 5- and 15-LOX-1-mediated SPM, such as RvD5, was not affected in M2-MDMs by compound **6**, indicating that 5-LOX activity for SPM biosynthesis is not impaired (Fig. 6D). Moreover, compound **6** elicited a differential modulation of COX-derived LMs where thromboxane B_2 (TXB_2) levels were significantly reduced but PGs, including PGE_2, PGD_2, and $PGF_{2\alpha}$, were markedly elevated (Fig. 6D–F). These findings suggest a redirection of AA metabolism from the 5-LOX pathway toward enhanced COX pathway activity, along with suppression of TX formation.

2.4. Compound 6 modulates lipid mediator biosynthesis in murine zymosan-induced peritonitis

To evaluate the effect of compound **6** on 5-LOX/FLAP and sEH product formation *in vivo*, we employed a well-established experimental model of LM-driven inflammation, namely zymosan-induced peritonitis in mice. Male mice were pre-treated intraperitoneally with compound **6** (10 mg/kg), followed 30 min later by zymosan administration (1 mg/mouse) (Fig. 7A). 4 h post-zymosan injection, mice were euthanized, and LMs were quantified in peritoneal exudates using UPLC-MS/MS. To measure the plasmatic concentration of compound **6** during the zymosan-induced peritonitis, we performed LC-MS/MS analysis. 4 h after intraperitoneal administration of compound **6** at a dose of 10 mg/kg, the plasma concentration was 32.26 ± 4.45 ng mL^{-1} ($n = 5$). These findings indicate that compound **6** is systemically available at this time point, suggesting sustained plasma levels following administration.

Compound **6** clearly modulated specific pro-inflammatory and anti-inflammatory LM levels in the exudates. In this context, as observed in the *in vitro* experiments, pre-treatment of mice with compound **6** led to a significant reduction of AA-derived 5-LOX/FLAP products induced by zymosan (Fig. 7B). Specifically, the levels of LTB_4, 5-HETE, and LTE_4 were markedly reduced in the mice treated with compound **6** (Fig. 7B and C), while the level of EPA-derived 5-HEPE was not altered (Fig. 7B).

It is well established that inhibition of sEH results in elevated levels of anti-inflammatory EETs and in a corresponding decrease of pro-inflammatory DHETs, thereby attenuating inflammation in both acute and chronic experimental models. LM analysis showed that treatment with compound **6** led to an increase in the EET/DHET ratio (Fig. 7D), driven by elevated anti-inflammatory EET levels (Fig. 7B and C), particularly 11,12-EET and 14,15-EET (Fig. 7B) and a concomitant decrease in pro-inflammatory DHETs (Fig. 7C), such as 11,12-DHET (Fig. 7B) in the exudates, confirming sEH as target of compound **6**. In addition, a significant reduction of PG levels induced by zymosan injection was observed, especially PGE_2, while no effects on TXB_2 were obvious (Fig. 7B and C). Moreover, compound **6** did not impact the production of AA- and EPA-derived 12-/15-LOX products (Fig. 7B).

Collectively, these findings demonstrate that compound **6** effectively modulates key inflammatory pathways *in vivo* by targeting FLAP– and sEH–dependent LM biosynthesis, leading to a shift from pro-inflammatory (LTs and DHETs) to anti-inflammatory mediator profiles (EETs).

3. Conclusion

In this report, we reveal compound **6** as dual FLAP/sEH inhibitor with *in vivo* activity. The discovery of this lead compound originated from an *in-silico* study that addressed the identification of the chemical requirements needed to effectively and simultaneously bind both FLAP and sEH proteins, thereby reducing pro-inflammatory LM production while preserving the levels of anti-inflammatory LMs. By integrating the analysis of the *in vitro* results with molecular modelling information, we successfully achieved our goal (see Fig. 5), obtaining clear insights into the structural motifs that orient the affinity of **6** to FLAP and sEH and at the same time reducing the interaction with 5-LOX, thus preserving 5-LOX-dependent SPM biosynthesis. This approach will be helpful in the future design of multitarget LM pathway modulators, rationalizing their molecular architecture in accordance with the desired activity.

To the best of our knowledge, few examples for FLAP/sEH multiple inhibitors exist, all structurally related to diflapolin. This underscores the medicinal chemistry potential of this underexplored area, where defining the structural requirements for dual activity is a critical step toward the rational design of such inhibitors.

Multitarget approaches in the inflammatory field are well-recognized strategies. The complexity degree of the inflammatory process, as in term of involved proteins and mediators, as well as for the biological repercussions, makes the multiple inhibition principle an advantageous option. This is evident in terms of reduction of side effects, increasing of therapeutic efficacy and decreasing of unfavourable compensatory effects [41].

The *in vivo* characterization of derivative **6** highlighted a very clear trend in the rearrangement of LMs detected by UPLC-MS/MS-based metabololipidomics. The reduction of LTs and DHET levels and the enhanced levels of EETs underlines the favourable profile of LMs following compound **6** administration to mice. These results make derivative **6** a valuable hit compound for further developments of FLAP/sEH inhibitors as multitarget agents for exploitation in acute and chronic inflammatory diseases.

4. Experimental section

4.1. Experimental section

General: All the other reagents and solvents were purchased from Merck (Milan, Italy), unless otherwise stated. Reactions were performed under magnetic stirring in round-bottomed flasks unless otherwise noted. Moisture-sensitive reactions were conducted in oven-dried glassware under nitrogen stream, using freshly distilled solvents. TLC analysis of reaction mixtures was performed on precoated glass silica gel plates (F254, 0.25 mm, VWR International), while crude products were purified by the Isolera Spektra One automated flash chromatography system (Biotage, Uppsala, Sweden), using commercial silica gel cartridges (SNAP KP-Sil, Biotage). NMR spectra were recorded on a Bruker

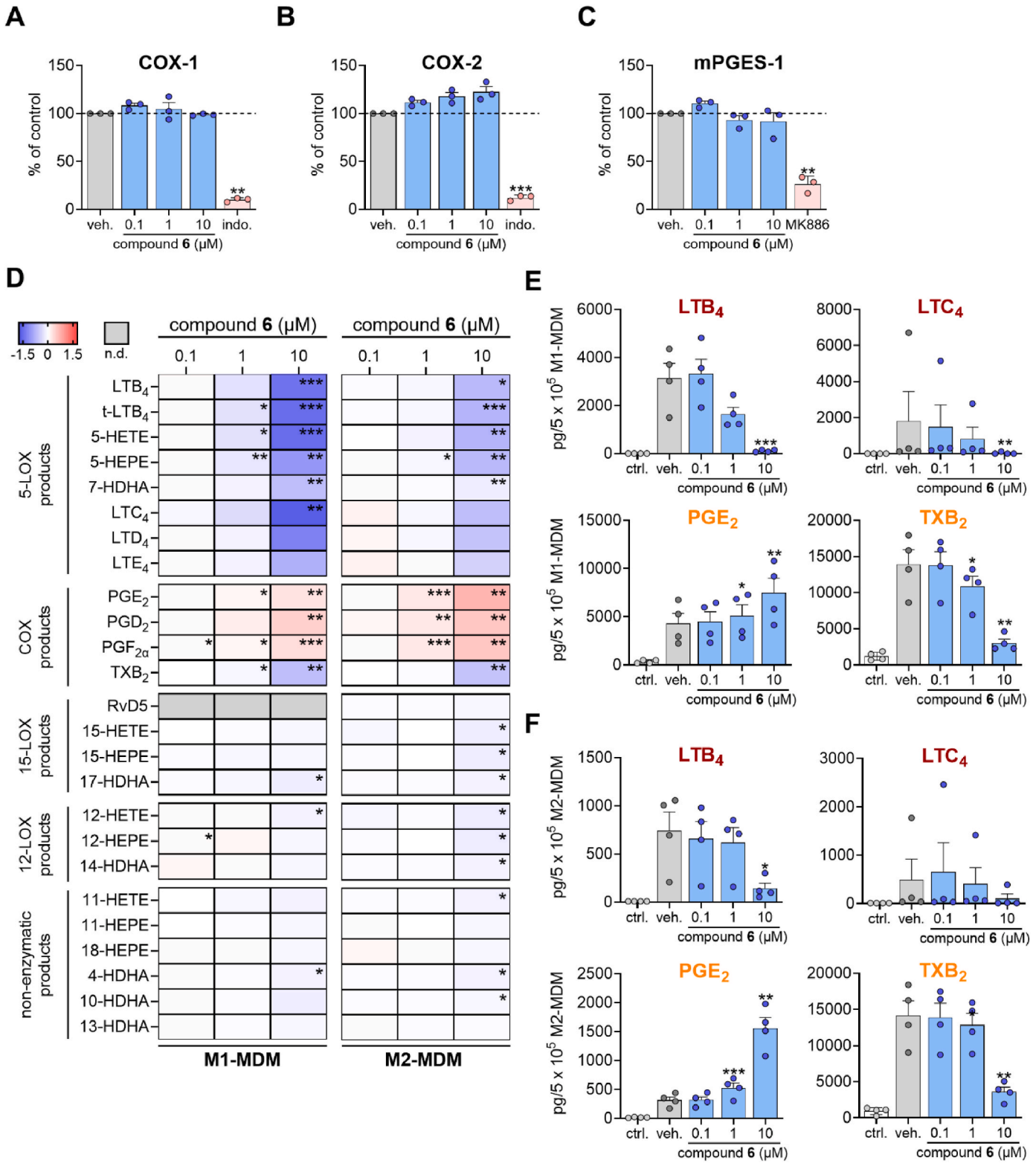

Fig. 6. Effects of compound **6** on isolated enzymes and LMs formation in human macrophages. (**A**) Isolated ovine COX-1, (**B**) human recombinant COX-2, and as well as, (**C**) mPGES-1 in microsomal preparations of IL-1β-stimulated A549 cells, were incubated with the vehicle (0.1 % DMSO) as the control (=100 %), 0.1, 1 or 10 μM of compound **6**, or control inhibitors such as 10 μM indomethacin (indo.) for COX-1/2 and MK886 (10 μM) for mPGES-1, and the enzymatic activities were assessed. Data are given as % of control ±SEM, $n = 3$. One-way ANOVA with Dunnett's multiple comparisons test against veh., $^{**}p < 0.01$, $^{***}p < 0.001$. (**D-F**) M1-and M2-MDMs were treated with vehicle (veh., 0.1 % DMSO) or compound **6** at the indicated concentrations for 30 min and then stimulated with 1 % SACM for 90 min. (**D**) LM formation is shown as log data of -fold change versus vehicle-treated controls in a heatmap, $n = 4$. Results for selected LMs of M1-MDMs (**E**) and M2-MDMs (**F**) are shown as pg/5 × 10^5 cells as mean ± SEM in bar charts, $n = 4$, one-way ANOVA with Dunnett's multiple comparison test against veh.-treated cells, $^{*}p < 0.05$, $^{**}p < 0.01$, $^{***}p < 0.001$.

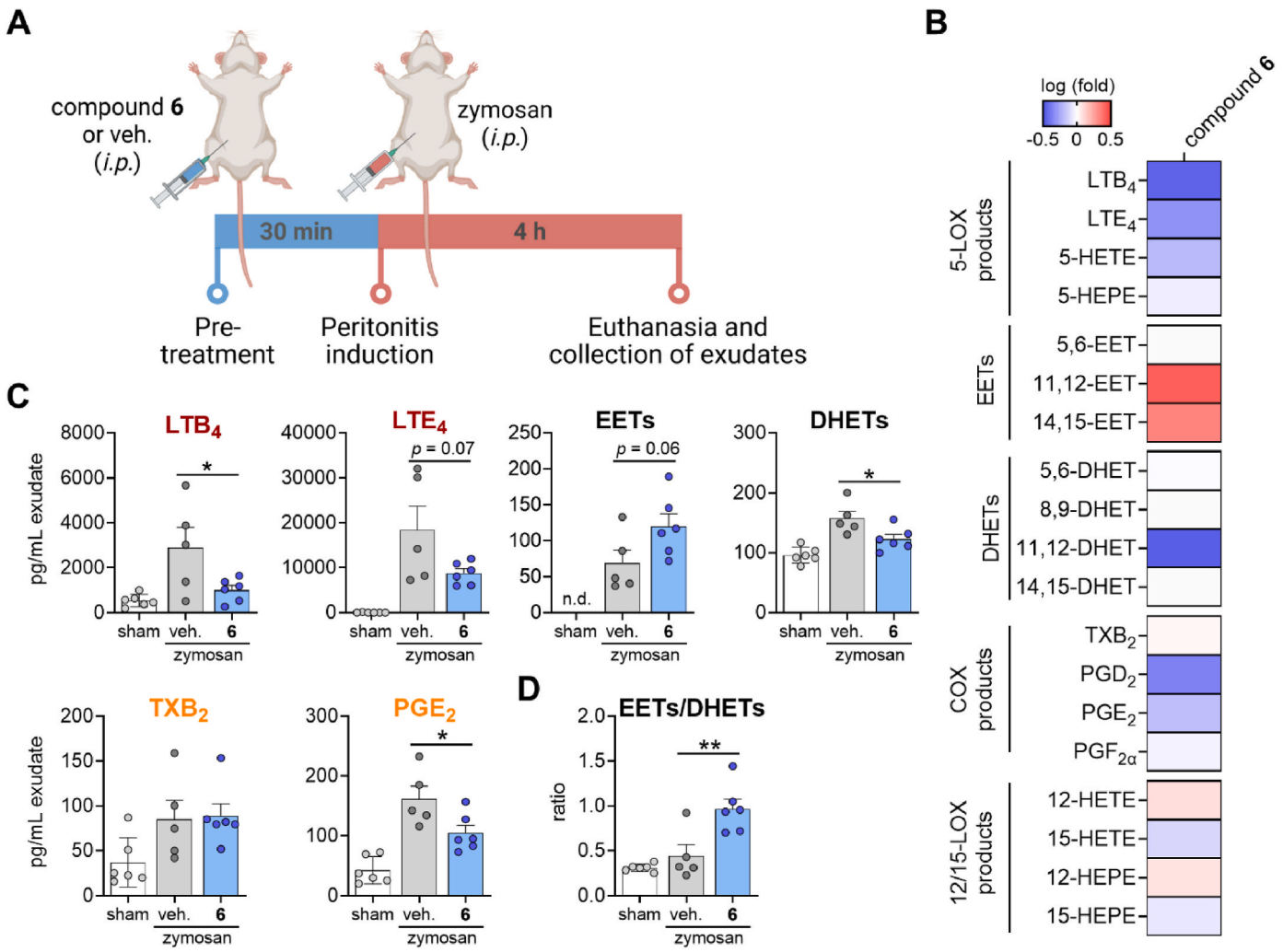

Fig. 7. Effects of compound **6** on LM formation in murine peritonitis. (**A**) Experimental timeline of zymosan-induced mouse peritonitis. Mice received compound **6** (10 mg/kg; zymosan + **6** group) or vehicle (0.5 mL PBS with 2 % DMSO, 3 % Tween 20, and 3 % PEG 400, veh. group) *i.p.*, 30 min prior to induction of peritonitis by zymosan (1 mg/mouse, *i.p.*). After 4 h, peritoneal exudates were collected. (**B-D**) LMs were extracted from the exudates and analyzed by UPLC-MS/MS. (**B**) LMs levels are shown as log data of -fold changes of compound **6**-treated mice against the vehicle-treated mice in a heatmap, $n = 5$–6. (**C**) Results for selected 5-LOX/FLAP products (LTB_4, LTE_4), COX products (TXB_2, PGE_2), as well as EETs (sum of 5,6-EET, 11,12-EET and 13,15-EET) and DHETs (sum of 5,6-DHET, 8,9-DHET, 11,12-DHET and 14,15-DHET) are shown for sham controls, vehicle-treated and compound **6**-treated mice as pg/mL exudate as means ± SEM in bar charts, $n = 5$–6. One-way ANOVA with Tukey's multiple comparison test, $^*p < 0.05$, $^{**}p < 0.01$. (**D**) Ratio of the sum of EETs against the sum of DHETs is shown as mean ± SEM in bar charts, $n = 5$–6. One-way ANOVA with Tukey's multiple comparison test, $^{**}p < 0.01$.

Avance 400 MHz apparatus, at room temperature. Chemical shifts were reported in δ values (ppm) relative to internal Me_4Si for ^1H and ^{13}C NMR. J values were reported in hertz (Hz). ^1H NMR peaks were described using the following abbreviations: s (singlet), d (doublet), t (triplet), and m (multiplet). HR-MS spectra were recorded by LTQ-Orbitrap-XL-ETD mass spectrometer (Thermo Scientific, Bremen, Germany), equipped with an ESI source. All the final compounds showed a purity ≥95 % as assessed by RP-UHPLC-PDA analysis, performed using a Nexera UHPLC system (Shimadzu, Kyoto, Japan) consisting of a CBM-40 lite controller, two LC-40B X3 pumps, an SPD-M 40 photo diode array detector, a CTO-30A column oven and, a SIL-40C X3 autosampler. The chromatographic analysis was accomplished on a Kinetex® Evo C18 column, 150 × 2.1 mm × 2.6 μm (Phenomenex®, Bologna, Italy) maintained at 40 °C. The optimal mobile phase consisted of 0.1 % $HCOOH/H_2O$ v/v (A) and 0.1 % HCOOH/ACN v/v (B) delivered at constant flow rate of 0.3 mL/min $^{-1}$. Analysis was performed in gradient elution as follows: 0–20.00 min, 5–95 % B; 20.00–25.00 min, isocratic to 95 % B; then 5 min for column re-equilibration. Data acquisition was set in the range 190–800 nm and chromatograms were monitored at 254 nm.

4.2. General procedure A: Pd-catalysed reduction and deprotection reaction (b, 6, 7, 10, n, 14, t)

To a solution of starting material (1.0 mmol) in a mixture of THF/MeOH (1/1 v/v), ammonium formate (10 eq) and Pd/C (10 % mol) were added. The reaction mixture was refluxed at 110 °C until the complete disappearance of the starting material, monitored by TLC. After completion, the reaction solution was filtered through Celite 503 (Merck Millipore, Burlington, USA) and evaporated under vacuum, yielding the final compounds or the corresponding intermediates that were used in the next step without further purification.

4.3. General procedure B: urea formation (c, d, j, k, o, p, u, v)

To a solution of 1,4-phenylenediamine, 4-aminobenzylamine, intermediate **b**, **i**, **n** or **t** (0.1 mmol) in dichloromethane, triphosgene (0.4 eq), triethylamine (1.2 eq) and the proper amine (1.2 eq) were added

and the mixture was stirred for 1 h at room temperature. After the completion of the reaction, monitored by TLC, water (30 mL) was added and the mixture was extracted with dichloromethane (3 x 10 mL); the organic layer was dried over Na_2SO_4, filtered and evaporated. Flash chromatography using n-hexane/ethyl acetate as mobile phase furnished the corresponding urea compounds.

4.4. General procedure C: hydrolysis (e, f, 8, 12, 13, 15, 16)

The proper ester intermediate (1 mmol) was dissolved in methanol (5 mL) and added with 2 mL of NaOH 1 M aqueous solution. The reaction mixture was stirred at 100 °C until the complete disappearance of the starting material, evidenced by TLC. The aqueous phase was quenched with 20 mL of HCl 2 M, diluted with ethyl acetate and extracted. Then, the organic layer was filtered, dried over anhydrous Na_2SO_4 and evaporated in vacuo affording the final derivatives without further purification.

4.5. General procedure D: coupling reaction (1–5)

To a solution of **e** or **f** (1.0 mmol) in dichloromethane, methyl 4-aminobutyrate, methyl 4-(aminomethyl)benzoate, 4-nitrobenzylamine, benzylamine, 1-propylamine or 2-(4-biphenyl)ethylamine(1.2 mmol), HOBt (1.2 mmol), HBTU (1.2 mmol) and DIPEA (2.4 mmol) were added and the mixture was stirred at room temperature for 12 h. Afterward, the reaction mixture was diluted with dichloromethane (20 mL), and the resulting solution was washed successively with 10 % aqueous solution of citric acid (2 × 15 mL), 10 % aqueous solution of $NaHCO_3$ (2 × 15 mL), and water (2 × 15 mL). The organic phase was dried over Na_2SO_4, filtered and concentrated in vacuo. Flash chromatography of the residues, using mixtures of dichloromethane/ethyl acetate as eluent system furnished the corresponding amide derivatives.

4.6. General procedure E: reductive amination (h, w)

To a solution of 2-nitro-1,4-phenylendiamine or intermediate **v** (0.1 mmol) in DCM/CH_3COOH (5:1 v/v) 1.2 eq of methyl 4-formylbenzoate were added and the mixture was stirred at 80 °C. After 3 h sodium triacetoxyborohydride (1.8 eq) was added portionwise and the mixture was refluxed for further 1 h. After cooling to room temperature, 20 mL of NaOH 1 N solution were added and the organic layer was separated. Then it was dried over Na_2SO_4, filtered, and concentrated under vacuum. Flash chromatography on silica gel using n-hexane/ethyl acetate (4:1, v:v) as mobile phase furnished intermediate **h** or **w**.

4.7. General procedure F: alkylation reaction (9, l, 11, q, r)

Intermediate **k**, deprotected **o** or **p** (0.1 mmol) was dissolved in acetonitrile and added with 2 equivalents of potassium *tert*-butoxide and 2 equivalents of the proper alkyl halide. Afterward, the mixture was heated to 120 °C in a microwave reactor for 1 h, quenched by 10 % aqueous solution of citric acid and diluted with dichloromethane. The organic layer was separated, dried over anhydrous Na_2SO_4, filtered, and concentrated under vacuum. Flash chromatography of the crude mixture using n-hexane/ethyl acetate as mobile phase furnished the purified intermediates.

4.8. General procedure G: Boc removal (11.1-r.1)

The *N*-Boc protected intermediates **o** or **p** (1 mmol) were dissolved in a mixture of TFA/DCM (1/3, v/v), and triisopropylsilane (TIS, 0.25 mmol) was added. The mixture was stirred at room temperature for 3 h. Then, a solution of NaOH (2 N) was added until pH 7. The mixtures were diluted with dichloromethane, and the organic phase was extracted, dried over Na_2SO_4, filtered, and concentrated in vacuo. The final products were obtained by precipitation from dichloromethane and diethyl ether.

4.9. Synthesis of methyl 2,4-dinitrobenzoate (a)

To a 10 mL microwave vial charged with methanol (6 mL) and a magnetic stir bar 2,4-dinitrobenzoic acid (1 mmol) was added. The reaction vessel was sealed and heated under microwave irradiation for 1 h at 110 °C. After cooling, the reaction vessel was uncapped, the vial content evaporated and diluted with dichloromethane and 20 mL of NaOH 1 M aqueous solution. Upon the extraction, the organic layer was dried over anhydrous Na_2SO_4, filtered, and evaporated under vacuum. The resulting crude was used in the next step without further purification step. Whitish powder (98 % yield). ^{1}H NMR (400 MHz, $CDCl_3$): δ: 4.01 (s, 3H, CH_3); 7.97 (d, 1H, aryl, J = 8.4 Hz); 8.56 (d, 1H, aryl, J = 10.5 Hz); 8.81 (s, 1H, aryl).

4.10. Methyl 2,4-diaminobenzoate (b)

Obtained from **a** following the general procedure A. Whitish powder (94 % yield). ^{1}H NMR (400 MHz, CD_3OD): δ: 3.77 (s, 3H, CH_3); 5.95–5.98 (m, 2H, aryl); 7.56 (d, 1H, aryl, J = 8.6 Hz). HR-MS *m/z* calcd for $C_8H_{10}N_2O_2$ $[(M + H)]^+$: 167.0815; found 167.0844.

4.11. Methyl 2-amino-4-(3-(cyclohexylmethyl)ureido)benzoate (c)

Synthesized from **b** and cyclohexanemethylamine following the general procedure B. FC in n-hexane/ethyl acetate 1/1, R*f*: 0.45. Whitish powder (43 % yield). ^{1}H NMR (400 MHz, CD_3OD): δ: 0.92–1.02 (m, 2H, CH_2); 1.20–1.28 (m, 2H, CH_2); 1.69–1.83 (m, 5H, CH and CH_2); 1.89–1.94 (m, 2H, CH_2); 3.00 (d, 2H, CH_2, J = 8.1 Hz); 3.64 (s, 3H, CH_3); 6.33 (d, 1H, aryl, J = 10.6 Hz); 7.40 (d, 1H, aryl, J = 8.6 Hz); 7.52 (s, 1H, aryl). HR-MS *m/z* calcd for $C_{16}H_{23}N_3O_3$ $[(M + H)]^+$: 306.1812; found 306.1805.

4.12. Methyl 4-(3-(((3r,5r,7r)-adamantan-1-yl)methyl)ureido)-2-aminobenzoate (d)

Obtained from **b** and 1-adamantanemethylamine according to the general procedure B. FC in n-hexane/ethyl acetate 3/7, R*f*: 0.46. Whitish powder (53 % yield). ^{1}H NMR (400 MHz, CD_3OD): δ: 1.57 (s, 6H, CH_2); 1.72 (d, 3H, CH and CH_2, J = 11.6 Hz); 1.81 (d, 3H, CH and CH_2, J = 11.9 Hz); 2.00 (bs, 3H, CH and CH_2); 2.90 (s, 2H, CH_2); 3.82 (s, 3H, CH_3); 6.49 (d, 1H, aryl, J = 10.8 Hz); 6.97 (s, 1H, aryl); 7.69 (d, 1H, aryl, J = 8.8 Hz). HR-MS *m/z* calcd for $C_{20}H_{27}N_3O_3$ $[(M + H)]^+$: 358.2125; found 358.2177.

4.13. 2-Amino-4-(3-(cyclohexylmethyl)ureido)benzoic acid (e)

Intermediate **e** was obtained from **c** following the general procedure C. Whitish powder (95 % yield). ^{1}H NMR (400 MHz, CD_3OD): δ: ^{1}H NMR (400 MHz, CD_3OD): δ: 0.94–1.05 (m, 2H, CH_2); 1.21–1.28 (m, 2H, CH_2); 1.68–1.84 (m, 5H, CH and CH_2); 1.90–1.95 (m, 2H, CH_2); 3.02 (d, 2H, CH_2, J = 8.2 Hz); 6.40 (d, 1H, aryl, J = 10.4 Hz); 7.44 (d, 1H, aryl, J = 8.5 Hz); 7.57 (s, 1H, aryl). HR-MS *m/z* calcd for $C_{15}H_{21}N_3O_3$ $[(M + H)]^+$: 292.1656; found 292.1659.

4.14. 4-(3-(((3r,5r,7r)-adamantan-1-yl)methyl)ureido)-2-aminobenzoic acid (f)

Obtained from **d** following the general procedure C. Whitish powder (93 % yield). ^{1}H NMR (400 MHz, CD_3OD): δ: 1.57 (s, 6H, CH_2); 1.71 (d, 3H, CH and CH_2, J = 11.6 Hz); 1.80 (d, 3H, CH and CH_2, J = 11.9 Hz); 2.00 (bs, 3H, CH and CH_2); 2.91 (s, 2H, CH_2); 3.82 (s, 3H, CH_3); 6.49 (d, 1H, aryl, J = 8.7 Hz); 6.95 (s, 1H, aryl); 7.71 (d, 1H, aryl, J = 8.7 Hz). HR-MS *m/z* calcd for $C_{19}H_{25}N_3O_3$ $[(M + H)]^+$: 344.1969; found 344.1980.

4.15. Methyl 4-(2-amino-4-(3-(cyclohexylmethyl)ureido)benzamido) butanoate [1]

Synthesized from **e** and methyl 4-aminobutyrate according to the general procedure D. FC in n-hexane/ethyl acetate 1/1, Rf: 0.46. Whitish oil (52 % yield). ^{1}H NMR (400 MHz, CD_3OD): δ: 0.92–1.02 (m, 2H, CH_2); 1.20–1.28 (m, 2H, CH_2); 1.69–1.83 (m, 7H, CH and CH_2); 1.89–1.94 (m, 2H, CH_2); 2.42 (t, 2H, CH_2, J = 7.3 Hz); 3.03 (d, 2H, CH_2, J = 6.8 Hz); 3.37 (t, 2H, CH_2, J = 6.9 Hz); 3.66 (s, 3H, CH_3); 6.29 (d, 1H, aryl, J = 10.8 Hz); 7.37 (d, 1H, aryl, J = 8.6 Hz); 7.50 (s, 1H, aryl). ^{13}C NMR (100 MHz, CD_3OD) δ: 28.4, 36.7, 39.9, 47.3, 51.1, 51.2, 54.7, 104.5, 110.4, 113.1, 126.9, 128.5, 129.3, 129.33, 133.9, 146.3, 147.3, 157.9, 167.1. HR-MS *m/z* calcd for $C_{28}H_{35}N_3O_4$ [(M + H)]$^+$: 391.2340; found 391.2335.

4.16. Methyl 4-((4-(3-(adamantan-1-ylmethyl)ureido)-2-aminobenzamido)methyl)benzoate (2)

Obtained from **f** and methyl 4-(bromomethyl)benzoate according to the general procedure D. FC in n-hexane/ethyl acetate 7/3, Rf: 0.47. Yellowish oil (64 % yield). ^{1}H NMR (400 MHz, CD_3OD): δ: 1.53 (s, 6H, CH_2); 1.66 (d, 3H, CH and CH_2, J = 11.8 Hz); 1.78 (d, 3H, CH and CH_2, J = 12.0 Hz); 1.95 (bs, 3H, CH and CH_2); 2.86 (s, 2H, CH_2); 3.90 (s, 3H, CH_3); 4.58 (s, 2H, CH_2); 6.31 (dd, 1H, aryl, J' = 2.3 Hz, J'' = 8.6 Hz); 7.43–7.48 (m, 3H, aryl); 7.52 (s, 1H, aryl); 7.97 (d, 2H, aryl, J = 8.3 Hz). ^{13}C NMR (100 MHz, DMSO) δ: 28.4, 33.8, 36.7, 39.9, 42.5, 51.2, 104.6, 107.3, 108.2, 126.9, 128.6, 128.9, 129.3, 142.6, 145.1, 152.1, 156.8, 167.0, 170.2. HR-MS *m/z* calcd for $C_{28}H_{34}N_4O_4$ [(M + H)]$^+$: 491.2653; found 491.2633.

4.17. 4-(3-(((3r,5r,7r)-adamantan-1-yl)methyl)ureido)-2-amino-N-(4-nitrobenzyl)benzamide (g)

Synthesized from **f** and 4-nitrobenzylamine following the general procedure D. FC in n-hexane/ethyl acetate 8/2, Rf: 0.44. Yellowish oil (60 % yield). ^{1}H NMR (400 MHz, CD_3OD): δ: 1.57 (s, 6H, CH_2); 1.70 (d, 3H, CH and CH_2, J = 12.3 Hz); 1.78 (d, 3H, CH and CH_2, J = 12.1 Hz); 2.00 (bs, 3H, CH and CH_2); 2.90 (s, 2H, CH_2); 4.63 (s, 2H, CH_2); 6.66 (dd, 1H, aryl, J' = 2.1 Hz and J'' = 8.7 Hz); 6.88 (d, 2H, aryl, J = 2.1 Hz); 7.48 (d, 1H, aryl, J = 8.7 Hz); 7.58 (d, 2H, aryl, J = 8.7 Hz); 8.22 (d, 2H, aryl, J = 8.7 Hz); 7.38 (d, 1H, aryl, J = 8.3 Hz). HR-MS *m/z* calcd for $C_{26}H_{31}N_5O_4$ [(M + H)]$^+$: 477.2376; found 477.2398.

4.18. 4-(3-(adamantan-1-ylmethyl)ureido)-2-amino-N-benzylbenzamide [3]

Obtained from **f** and benzylamine according to the general procedure D. FC in n-hexane/ethyl acetate hexane/ethyl acetate 1/1. Rf: 0.42. Yellowish powder (62 % yield). ^{1}H NMR (400 MHz, CD_3OD): δ: 1.56 (s, 6H, CH_2); 1.70 (d, 3H, CH and CH_2, J = 11.8 Hz); 1.78 (d, 3H, CH and CH_2, J = 12.1 Hz); 2.00 (bs, 3H, CH and CH_2); 2.90 (s, 2H, CH_2); 4.53 (s, 2H, CH_2); 6.65 (dd, 1H, aryl, J' = 2.1 Hz and J'' = 8.7 Hz); 6.87 (d, 1H, aryl, J = 2.1 Hz); 7.22–7.26 (m, 1H, aryl); 7.31–7.36 (m, 4H, aryl); 7.43 (d, 1H, aryl, J = 8.6 Hz). ^{13}C NMR (100 MHz, CD_3OD) δ: 28.4, 33.5, 36.7, 39.8, 42.5, 51.0, 104.9, 106.7, 109.8, 126.6, 126.9, 128.1, 128.6, 139.3, 143.6, 150.4, 156.7, 170.2. HR-MS *m/z* calcd for $C_{26}H_{32}N_4O_2$ [(M + H)]$^+$: 433.2598; found 433.2576.

4.19. 4-(3-(adamantan-1-ylmethyl)ureido)-2-amino-N-propylbenzamide [4]

Obtained from **f** and 1-propylamine according to the general procedure D. FC in n-hexane/ethyl acetate 3/7. Rf: 0.40. Yellowish powder (66 % yield). ^{1}H NMR (400 MHz, CD_3OD): δ: 0.99 (t, 3H, CH_3, J = 6.0 Hz); 1.58 (s, 6H, CH_2); 1.64 (dd, 1H, CH_2, J' = 5.8 Hz and J'' = 11.6 Hz); 1.71 (d, 3H, CH and CH_2, J = 9.3 Hz); 1.78 (d, 3H, CH and CH_2, J = 9.6 Hz); 1.99 (bs, 3H, CH and CH_2); 2.90 (s, 2H, CH_2); 3.30 (t, 2H, CH_2, J = 5.8 Hz); 6.31 (dd, 1H, aryl, J' = 1.8 Hz and J'' = 6.8 Hz); 7.38 (d, 1H, aryl, J = 6.8 Hz); 7.49 (bs, 1H, aryl). ^{13}C NMR (100 MHz, CD_3OD) δ: 10.4, 22.4, 28.4, 33.8, 36.7, 39.9, 41.0, 51.4, 104.9, 107.4, 109.3, 128.8, 142.0, 151.7, 156.9, 170.3. HR-MS *m/z* calcd for C22H32N$_4$O$_2$ [(M + H)]$^+$: 385.2598; found 385.2582.

4.20. N-(2-([1,1′-biphenyl]-4-yl)ethyl)-4-(3-(adamantan-1-ylmethyl) ureido)-2-aminobenzamide [5]

Obtained from **f** and 2-(4-biphenyl)ethylamine according to the general procedure D. FC in n-hexane/ethyl acetate hexane/ethyl acetate 1/1. Rf: 0.43. Yellowish powder (57 % yield). ^{1}H NMR (400 MHz, CD_3OD): δ: 1.58 (s, 6H, CH_2); 1.70 (d, 3H, CH and CH_2, J = 9.2 Hz); 1.78 (d, 3H, CH and CH_2, J = 9.6 Hz); 1.98 (bs, 3H, CH and CH_2); 2.96 (t, 2H, CH_2, J = 6.1 Hz); 3.60 (t, 2H, CH_2, J = 6.1 Hz); 6.29 (dd, 1H, aryl, J' = 1.8 Hz and J'' = 6.8 Hz); 7.31–7.36 (m, 4H, aryl); 7.44 (t, 2H, aryl, J = 6.4 Hz); 7.51 (bs, 1H, aryl); 7.57 (d, 2H, aryl, J = 6.6 Hz); 7.61 (d, 1H, aryl, J = 5.7 Hz). ^{13}C NMR (100 MHz, CD_3OD) δ: 28.4, 33.8, 35.0, 36.7, 39.9, 40.9, 51.3, 104.8, 107.3, 126.4, 126.6, 126.7, 128.4, 128.8, 129.0, 138.6, 139.1, 140.9, 142.1, 151.8, 156.9, 170.3. HR-MS *m/z* calcd for $C_{33}H_{38}N_4O_2$ [(M + H)]$^+$: 523.3068; found 523.3049.

4.21. 4-(3-(adamantan-1-ylmethyl)ureido)-2-amino-N-(4-aminobenzyl) benzamide [6]

Obtained from **g** according to the general procedure A. FC in n-hexane/ethyl acetate 1/9. Rf: 0.40. Yellowish powder (55 % yield). ^{1}H NMR (400 MHz, CD_3OD): δ: 1.55 (s, 6H, CH_2); 1.69 (d, 3H, CH and CH_2, J = 11.7 Hz); 1.78 (d, 3H, CH and CH_2, J = 12.1 Hz); 1.99 (bs, 3H, CH and CH_2); 2.89 (s, 2H, CH_2); 4.39 (s, 2H, CH_2); 6.63 (dd, 1H, aryl, J' = 2.1 Hz and J'' = 6.6 Hz); 6.72 (d, 2H, aryl, J = 8.4 Hz); 6.86 (d, 1H, aryl, J = 2.0 Hz); 7.11 (d, 2H, aryl, J = 8.3 Hz); 7.38 (d, 1H, aryl, J = 8.3 Hz). ^{13}C NMR (100 MHz, CD_3OD) δ: 28.8, 33.5, 36.7, 39.8, 42.3, 51.0, 104.9, 106.8, 110.2, 115.3, 128.1, 128.6, 128.8, 143.5, 146.2, 150.2, 156.7, 170.0. HR-MS *m/z* calcd for $C_{26}H_{33}N_5O_2$ [(M + H)]$^+$: 448.2707; found 448.2701.

4.22. Methyl 4-(((4-amino-3-nitrophenyl)amino)methyl)benzoate (h)

Synthesized from 2-nitro-1,4-phenylendiamine and methyl 4-formylbenzoate following the general procedure E. FC in n-hexane/ethyl acetate 8/2, Rf: 0.45. Yellowish powder (75 % yield). ^{1}H NMR (400 MHz, CD_3OD): δ: 3.91 (s, 3H, CH_3); 4.37 (s, 2H, CH_2); 6.84 (d, 1H, aryl, J = 9.0 Hz); 6.99 (dd, 1H, aryl, J' = 2.7 Hz and J'' = 6.3 Hz); 7.11 (d, 1H, aryl, J = 2.7 Hz); 7.51 (d, 2H, aryl, J = 8.2 Hz); 7.99 (d, 2H, aryl, J = 8.2 Hz). HR-MS *m/z* calcd for $C_{15}H_{15}N_3O_4$ [(M + H)]$^+$: 302.1135; found 302.1166.

4.23. Synthesis of methyl 4-(((4-amino-3-nitrophenyl)((benzyloxy) carbonyl)amino)methyl)benzoate (i)

To a solution of intermediate **h** (0.5 mmol) in dichloromethane, DIPEA (1.2 eq) and benzyloxycarbonyl chloride (1.2 eq) were added. The reaction mixture was stirred for 2 h at room temperature. Then, the organic phase was added with water and extracted with dichloromethane (3 x 15 mL). The organic layer was separated, dried over anhydrous Na_2SO_4, filtered, and evaporated under vacuum. The crude was purified by flash chromatography using n-hexane/ethyl acetate (4:1, v:v) as eluent system, furnishing the corresponding protected intermediate **i**. Rf: 0.45. Yellowish oil (92 % yield). ^{1}H NMR (400 MHz, $CDCl_3$): δ: 3.93 (s, 3H, CH_3); 4.90 (s, 2H, CH_2); 5.20 (s, 2H, CH_2); 6.70 (d, 1H, aryl, J = 8.8 Hz); 7.28–7.35 (m, 8H, aryl); 7.93 (s, 1H, aryl); 7.97 (d, 2H, aryl, J = 8.2 Hz). HR-MS *m/z* calcd for $C_{23}H_{21}N_3O_6$ [(M + H)]$^+$: 436.1503; found 436.1583.

4.24. Methyl 4-(((4-(3-(((1s,3s)-adamantan-1-yl)methyl)ureido)-3-nitrophenyl)((benzyloxy)carbonyl)amino)methyl)benzoate (j)

Obtained from **i** and 1-adamantanemethylamine according to the general procedure C. FC in dichloromethane/ethyl acetate 9.5/0.5, R*f*: 0.45. Yellowish oil (56 % yield). ^{1}H NMR (400 MHz, $CDCl_3$): *δ*: 1.55 (s, 6H, CH_2); 1.67 (d, 3H, C*H* and CH_2, *J* = 11.7 Hz); 1.76 (d, 3H, C*H* and CH_2, *J* = 12.1 Hz); 1.96 (bs, 3H, C*H* and CH_2); 2.89 (s, 2H, CH_2); 3.88 (s, 3H, CH_3); 4.98 (s, 2H, CH_2); 5.19 (s, 2H, CH_2); 7.29–7.34 (m, 6H, aryl); 7.45 (d, 1H, N*H*, *J* = 8.2 Hz); 7.92 (d, 2H, aryl, *J* = 8.2 Hz); 7.97 (bs, 1H, N*H*); 8.31 (d, 2H, aryl, *J* = 9.2 Hz). HR-MS *m/z* calcd for $C_{35}H_{38}N_4O_7$ $[(M + H)]^+$: 627.2813; found 627.2845.

4.25. Methyl 4-(((4-(3-(adamantan-1-ylmethyl)ureido)-3-aminophenyl)amino)methyl)benzoate [7]

Synthesized from **j** applying the general procedure A. Whitish powder (94 % yield). ^{1}H NMR (400 MHz, CD_3OD): *δ*: 1.48 (s, 6H, CH_2); 1.66 (d, 3H, C*H* and CH_2, *J* = 11.8 Hz); 1.75 (d, 3H, C*H* and CH_2, *J* = 12.1 Hz); 1.95 (bs, 3H, C*H* and CH_2); 2.84 (s, 2H, CH_2); 4.38 (s, 2H, CH_2); 6.06 (d, 1H, aryl, *J* = 11.0 Hz); 6.12 (d, 1H, aryl, *J* = 2.4 Hz); 6.78 (d, 1H, aryl, *J* = 8.4 Hz); 7.47 (d, 2H, aryl, *J* = 8.2 Hz). 7.95 (d, 2H, aryl, *J* = 8.2 Hz). ^{13}C NMR (100 MHz, CD_3OD) *δ*: 28.4, 36.7, 39.8, 46.9, 51.1, 51.3, 100.0, 104.0, 126.9, 128.4, 128.6, 129.2, 144.6, 146.4, 148.3, 159.4, 167.1. HR-MS *m/z* calcd for $C_{27}H_{34}N_4O_3$ $[(M + H)]^+$: 463.2704; found 463.2694.

4.26. 4-(((4-(3-(adamantan-1-ylmethyl)ureido)-3-aminophenyl)amino)methyl)benzoic acid [8]

Final derivative was obtained from **7** following the general procedure C. Precipitated from MeOH/diethyl ether. Whitish powder (92 % yield). ^{1}H NMR (400 MHz, CD_3OD): *δ*: 1.55 (s, 6H, CH_2); 1.69 (d, 3H, C*H* and CH_2, *J* = 11.7 Hz); 1.78 (d, 3H, C*H* and CH_2, *J* = 12.1 Hz); 1.98 (bs, 3H, C*H* and CH_2); 2.89 (s, 2H, CH_2); 4.43 (s, 2H, CH_2); 6.96 (d, 1H, aryl, *J* = 9.1 Hz); 7.20 (d, 1H, aryl, *J* = 2.8 Hz); 7.49 (d, 2H, aryl, *J* = 8.2 Hz); 7.79 (d, 1H, aryl, *J* = 9.1 Hz); 7.99 (d, 2H, aryl, *J* = 8.2 Hz). ^{13}C NMR (100 MHz, CD_3OD) *δ*: 28.4, 36.7, 39.9, 46.8, 51.4, 105.9, 119.8, 124.6, 125.4, 126.8, 129.6, 139.9, 144.3, 144.7, 156.9, 168.7. HR-MS *m/z* calcd for $C_{26}H_{32}N_4O_3$ $[(M + H)]^+$: 449.2547; found 449.2603.

4.27. 1-(((1s,3s)-adamantan-1-yl)methyl)-3-(4-aminophenyl)urea (k)

Obtained from 1,4-phenylenediamine and 1-adamantanemethylamine following the general procedure B. FC in n-hexane/ethyl acetate 3/7, R*f*: 0.48. Whitish powder (44 % yield). ^{1}H NMR (400 MHz, CD_3OD): *δ*: 1.55 (s, 6H, CH_2); 1.70 (d, 3H, C*H* and CH_2, *J* = 11.8 Hz); 1.78 (d, 3H, C*H* and CH_2, *J* = 12.1 Hz); 1.99 (bs, 3H, C*H* and CH_2); 2.89 (s, 2H, CH_2); 6.70 (d, 2H, aryl, *J* = 8.6 Hz); 7.08 (d, 2H, aryl, *J* = 8.6 Hz). HR-MS *m/z* calcd for $C_{18}H_{25}N_3O$ $[(M + H)]^+$: 300.2070; found 300.2055.

4.28. Methyl 4-(((4-(3-(adamantan-1-ylmethyl)ureido)phenyl)amino)methyl)benzoate [9]

Compound **9** was synthesized from **k** and methyl 4-(bromomethyl) benzoate according to the general procedure F. FC in n-hexane/ethyl acetate 1/1, R*f*: 0.45. Yellowish powder (54 % yield). ^{1}H NMR (400 MHz, CD_3OD): *δ*: 1.53 (s, 6H, CH_2); 1.68 (d, 3H, C*H* and CH_2, *J* = 11.7 Hz); 1.77 (d, 3H, C*H* and CH_2, *J* = 12.1 Hz); 1.98 (bs, 3H, C*H* and CH_2); 2.86 (s, 2H, CH_2); 3.90 (s, 3H, CH_3); 4.39 (s, 2H, CH_2); 6.58 (d, 2H, aryl, *J* = 8.8 Hz); 7.04 (d, 2H, aryl, *J* = 8.8 Hz); 7.48 (d, 2H, aryl, *J* = 8.2 Hz); 7.96 (d, 2H, aryl, *J* = 8.3 Hz). ^{13}C NMR (100 MHz, CD_3OD) *δ*: 28.4, 36.7, 39.8, 51.1, 51.2, 113.1, 122.5, 127.0, 128.4, 129.0, 129.2, 144.9, 146.3, 158.2, 167.1. HR-MS *m/z* calcd for $C_{27}H_{33}N_3O_3$ $[(M + H)]^+$: 448.2595; found 448.2590.

4.29. 1-(((1s,3s)-adamantan-1-yl)methyl)-3-(4-((4-nitrobenzyl)amino)phenyl)urea (l)

Obtained from **k** and 4-nitrobenzyl chloride following the general procedure F. FC in dichloromethane/ethyl acetate 9.5/0.5, R*f*: 0.45. Whitish oil (46 % yield). ^{1}H NMR (400 MHz, CD_3OD): *δ*: 1.53 (s, 6H, CH_2); 1.69 (d, 3H, C*H* and CH_2, *J* = 11.6 Hz); 1.78 (d, 3H, C*H* and CH_2, *J* = 12.1 Hz); 1.98 (bs, 3H, C*H* and CH_2); 2.87 (s, 2H, CH_2); 6.57 (d, 2H, aryl, *J* = 8.8 Hz); 7.05 (d, 2H, aryl, *J* = 8.8 Hz); 7.61 (d, 2H, aryl, *J* = 8.6 Hz); 8.19 (d, 2H, aryl, *J* = 8.7 Hz). HR-MS *m/z* calcd for $C_{25}H_{30}N_4O_3$ $[(M + H)]^+$: 435.2391; found 435.2380.

4.30. 1-(Adamantan-1-ylmethyl)-3-(4-((4-aminobenzyl)amino)phenyl)urea [10]

Final derivative **10** was synthesized from **l** applying the general procedure A. Precipitated from MeOH/diethyl ether. Whitish powder (51 % yield). ^{1}H NMR (400 MHz, CD_3OD): *δ*: 1.54 (s, 6H, CH_2); 1.69 (d, 3H, C*H* and CH_2, *J* = 11.6 Hz); 1.78 (d, 3H, C*H* and CH_2, *J* = 12.1 Hz); 1.99 (bs, 3H, C*H* and CH_2); 2.87 (s, 2H, CH_2); 4.14 (s, 2H, CH_2); 6.63 (d, 2H, aryl, *J* = 8.8 Hz); 6.70 (d, 2H, aryl, *J* = 8.4 Hz); 7.05 (d, 2H, aryl, *J* = 8.8 Hz); 7.12 (d, 2H, aryl, *J* = 8.3 Hz). ^{13}C NMR (100 MHz, DMSO) *δ*: 28.2, 37.1, 47.4, 51.3, 113.0, 114.2, 120.2, 127.6, 128.6, 130.2, 144.4, 147.8, 156.3. HR-MS *m/z* calcd for $C_{25}H_{32}N_4O$ $[(M + H)]^+$: 405.2649; found 405.2661.

4.31. Synthesis of tert-butyl (2-methoxy-4-nitrophenyl)carbamate m)

2-Methoxy-4-nitroaniline (0.5 mmol) was dissolved in dichloromethane, and added with DIPEA (1.5 eq) and di-*tert*-butyl dicarbonate (1.5 eq), and the mixture was refluxed overnight. Then, the organic phase was added with water and extracted with dichloromethane (3 x 15 mL). The organic layer was separated, dried over anhydrous Na_2SO_4, filtered, and evaporated under vacuum. The crude was purified by flash chromatography using n-hexane/ethyl acetate (4:1: v:v) as mobile phase, furnishing the corresponding protected intermediate **m**. R*f*: 0.47. Whitish powder (78 % yield). ^{1}H NMR (400 MHz, $CDCl_3$): *δ*: 1.57 (s, 9H, CH_3); 4.01 (s, 3H, CH_3); 7.37 (bs, 1H, N*H*); 7.75 (s, 1H, aryl); 7.94 (d, 1H, aryl, *J* = 9.0 Hz); 8.29 (d, 1H, aryl, *J* = 9.0 Hz). HR-MS *m/z* calcd for $C_{12}H_{16}N_2O_5$ $[(M + H)]^+$: 269.1132; found 269.1177.

4.32. Tert-butyl (4-amino-2-methoxyphenyl)carbamate (n)

Obtained from **m** following the general procedure A. Whitish powder (92 % yield). ^{1}H NMR (400 MHz, $CDCl_3$): *δ*: 1.53 (s, 9H, CH_3); 3.68 (bs, 2H, NH_2); 3.83 (s, 3H, CH_3); 6.35–6.40 (m, 2H, aryl); 6.79 (bs, 1H, N*H*); 7.81 (s, 1H, aryl). HR-MS *m/z* calcd for $C_{12}H_{18}N_2O_3$ $[(M + H)]^+$: 239.1390; found 239.1399.

4.33. Tert-butyl (4-(3-(((3r,5r,7r)-adamantan-1-yl)methyl)ureido)-2-methoxyphenyl)carbamate (o)

Intermediate **o** was synthesized from **n** and 1-adamantanemethylamine following the general procedure B. FC in dichloromethane/ethyl acetate 9.8/0.2, R*f*: 0.46. Yellowish powder (44 % yield). ^{1}H NMR (400 MHz, CD_3OD): *δ*: 1.52 (s, 9H, CH_3); 1.56 (s, 6H, CH_2); 1.70 (d, 3H, C*H* and CH_2, *J* = 9.2 Hz); 1.79 (d, 3H, C*H* and CH_2, *J* = 11.4 Hz); 1.99 (bs, 3H, C*H* and CH_2); 2.90 (s, 2H, CH_2); 3.86 (s, 3H, CH_3); 6.70 (d, 1H, aryl, *J* = 8.6 Hz); 7.30 (d, 1H, aryl, *J* = 8.4 Hz); 7.63 (d, 1H, aryl, *J* = 5.3 Hz); 7.12 (d, 2H, aryl, *J* = 8.3 Hz). HR-MS *m/z* calcd for $C_{24}H_{35}N_3O_4$ $[(M + H)]^+$: 430.2700; found 430.2763.

4.34. Tert-butyl (4-(3-cycloheptylureido)-2-methoxyphenyl)carbamate (p)

Obtained from **n** and cycloheptylamine applying the general

procedure B. FC in dichloromethane/ethyl acetate 9.8/0.2, R*f*: 0.46. Yellowish powder (51 % yield). ^{1}H NMR (400 MHz, CD_3OD): *δ*: 1.52 (s, 9H, C*H*$_3$); 1.55–1.68 (m, 8H, C*H*$_2$); 1.92–1.98 (m, 2H, C*H*$_2$); 3.79–3.83 (m, 1H, C*H*); 3.86 (s, 3H, C*H*$_3$); 6.69 (d, 1H, aryl, *J* = 6.4 Hz); 7.29 (d, 1H, aryl, *J* = 2.2 Hz); 7.61 (d, 1H, aryl, *J* = 7.4 Hz). HR-MS *m/z* calcd for $C_{20}H_{31}N_3O_4$ $[(M + H)]^+$: 378.2387; found 378.2375.

4.35. Methyl 4-(((4-(3-(adamantan-1-ylmethyl)ureido)-2-methoxyphenyl)amino)methyl)benzoate [11]

Final derivative **11** was obtained from deprotected **o** and methyl 4-(bromomethyl)benzoate following the general procedure F. FC in dichloromethane/ethyl acetate 9.5/0.5, R*f*: 0.45. Whitish powder (48 % yield). ^{1}H NMR (400 MHz, CD_3OD): *δ*: 1.54 (s, 6H, C*H*$_2$); 1.69 (d, 3H, C*H* and C*H*$_2$, *J* = 11.7 Hz); 1.78 (d, 3H, C*H* and C*H*$_2$, *J* = 12.0 Hz); 1.98 (bs, 3H, C*H* and C*H*$_2$); 2.87 (s, 2H, C*H*$_2$); 3.88 (s, 3H, C*H*$_3$); 3.90 (s, 3H, C*H*$_3$); 4.43 (s, 2H, C*H*$_2$); 6.40 (d, 1H, aryl, *J* = 8.4 Hz); 6.57 (d, 1H, aryl, *J* = 8.4 Hz); 7.01 (s, 1H, aryl); 7.46 (d, 2H, aryl, *J* = 8.1 Hz); 7.96 (d, 1H, aryl, *J* = 8.2 Hz). ^{13}C NMR (100 MHz, CD_3OD) *δ* 28.4, 36.7, 39.9, 47.3, 51.1, 51.2, 54.7, 104.5, 110.4, 113.1, 126.9, 128.5, 129.3, 129.33, 133.9, 146.3, 147.3, 157.9, 167.1. HR-MS *m/z* calcd for $C_{28}H_{35}N_3O_4$ $[(M + H)]^+$: 478.2700; found 478.2691.

4.36. Methyl 4-(((4-(3-cycloheptylureido)-2-methoxyphenyl)amino)methyl)benzoate (q)

Obtained from deprotected **p** and methyl 4-(bromomethyl)benzoate according to the general procedure F. FC in dichloromethane/ethyl acetate 9.5/0.5, R*f*: 0.47. Yellowish powder (45 % yield). ^{1}H NMR (400 MHz, $CDCl_3$): *δ*: 1.34–1.59 (m, 8H, C*H*$_2$); 1.89–1.93 (m, 2H, C*H*$_2$); 3.47–3.54 (m, 1H, C*H*); 3.85 (s, 3H, C*H*$_3$); 3.92 (s, 3H, C*H*$_3$); 4.84 (d, 1H, N*H*, *J* = 8.1 Hz); 6.37–6.41 (m, 2H, aryl and N*H*); 6.57 (d, 1H, aryl, *J* = 8.3 Hz); 6.88 (s, 1H, aryl); 7.44 (d, 2H, aryl, *J* = 8.2 Hz); 8.02 (d, 2H, aryl, *J* = 8.2 Hz). HR-MS *m/z* calcd for $C_{24}H_{31}N_3O_4$ $[(M + H)]^+$: 426.2387; found 426.2343.

4.37. 1-(((3r,5r,7r)-adamantan-1-yl)methyl)-3-(3-methoxy-4-((4-nitrobenzyl)amino)phenyl)urea (r)

Obtained from deprotected **o** and 4-nitrobenzyl chloride following the general procedure F. FC in dichloromethane/ethyl acetate 9.8/0.2, R*f*: 0.44. Whitish powder (50 % yield). ^{1}H NMR (400 MHz, CD_3OD): *δ*: 1.53 (s, 6H, C*H*$_2$); 1.67 (d, 3H, C*H* and C*H*$_2$, *J* = 11.7 Hz); 1.77 (d, 3H, C*H* and C*H*$_2$, *J* = 12.1 Hz); 1.97 (bs, 3H, C*H* and C*H*$_2$); 2.87 (s, 2H, C*H*$_2$); 3.89 (s, 3H, C*H*$_3$); 4.49 (s, 2H, C*H*$_2$); 6.35 (d, 1H, aryl, *J* = 8.4 Hz); 6.56 (d, 1H, aryl, *J* = 8.4 Hz); 7.02 (s, 1H, aryl); 7.58 (d, 2H, aryl, *J* = 8.7 Hz); 8.17 (d, 2H, aryl, *J* = 8.7 Hz). HR-MS *m/z* calcd for $C_{26}H_{32}N_4O_4$ $[(M + H)]^+$: 465.2496; found 465.2507.

4.38. 4-(((4-(3-(adamantan-1-ylmethyl)ureido)-2-methoxyphenyl)amino)methyl)benzoic acid [12]

Final compound **12** was obtained from **11** following the general procedure C. Precipitated from MeOH/diethyl ether. Whitish powder (92 % yield). ^{1}H NMR (400 MHz, CD_3OD): *δ*: 1.53 (s, 6H, C*H*$_2$); 1.68 (d, 3H, C*H* and C*H*$_2$, *J* = 11.7 Hz); 1.77 (d, 3H, C*H* and C*H*$_2$, *J* = 12.0 Hz); 1.97 (bs, 3H, C*H* and C*H*$_2$); 2.87 (s, 2H, C*H*$_2$); 3.87 (s, 3H, C*H*$_3$); 4.41 (s, 2H, C*H*$_2$); 6.42 (d, 1H, aryl, *J* = 8.4 Hz); 6.58 (d, 1H, aryl, *J* = 10.0 Hz); 7.01 (s, 1H, aryl); 7.43 (d, 2H, aryl, *J* = 8.0 Hz); 7.96 (d, 1H, aryl, *J* = 8.1 Hz). ^{13}C NMR (100 MHz, CD_3OD) *δ*: 28.4, 36.7, 39.9, 47.3, 51.2, 54.7, 104.4, 110.5, 113.2, 126.7, 129.4, 129.5, 130.1, 133.9, 145.5, 147.4, 158.0, 169.2. HR-MS *m/z* calcd for $C_{27}H_{33}N_3O_4$ $[(M + H)]^+$: 464.2544; found 464.2536.

4.39. 4-(((4-(3-cycloheptylureido)-2-methoxyphenyl)amino)methyl)benzoic acid [13]

Obtained from **q** applying the general procedure C. Precipitated from MeOH/diethyl ether. Whitish powder (95 % yield). ^{1}H NMR (400 MHz, CD_3OD): *δ*: 1.46–1.65 (m, 10H, C*H*$_2$); 1.90–1.95 (m, 2H, C*H*$_2$); 3.75–3.78 (m, 1H, C*H*); 3.88 (s, 3H, C*H*$_3$); 4.41 (s, 2H, C*H*$_{32}$); 6.42 (d, 1H, aryl, *J* = 8.4 Hz); 6.56 (d, 1H, aryl, *J* = 8.7 Hz); 7.01 (s, 1H, aryl); 7.43 (d, 2H, aryl, *J* = 8.1 Hz); 7.95 (d, 2H, aryl, *J* = 8.2 Hz). ^{13}C NMR (100 MHz, CD_3OD) *δ*: 23.7, 27.8, 35.1, 47.3, 50.6, 54.7, 104.3, 110.5, 113.0, 126.6, 129.3, 129.4, 131.0, 133.9, 145.1, 147.3, 156.8, 169.9. HR-MS *m/z* calcd for $C_{23}H_{29}N_3O_4$ $[(M + H)]^+$: 412.2231; found 412.2221.

4.40. 1-(Adamantan-1-ylmethyl)-3-(4-((4-aminobenzyl)amino)-3-methoxyphenyl)urea [14]

Final derivative **14** was synthesized from **r** following the general procedure A. Precipitated from MeOH/diethyl ether. Whitish powder (92 % yield). ^{1}H NMR (400 MHz, CD_3OD): *δ*: 1.55 (s, 6H, C*H*$_2$); 1.70 (d, 3H, C*H* and C*H*$_2$, *J* = 11.8 Hz); 1.78 (d, 3H, C*H* and C*H*$_2$, *J* = 12.1 Hz); 1.99 (bs, 3H, C*H* and C*H*$_2$); 2.88 (s, 2H, C*H*$_2$); 3.85 (s, 3H, C*H*$_3$); 4.16 (s, 2H, C*H*$_2$); 6.56 (d, 1H, aryl, *J* = 8.4 Hz); 6.61–6.64 (m, 1H, aryl); 6.70 (d, 2H, aryl, *J* = 8.3 Hz); 7.00 (d, 2H, aryl, *J* = 2.0 Hz); 7.11 (d, 2H, aryl, *J* = 8.2 Hz). ^{13}C NMR (100 MHz, CD_3OD) *δ*: 28.4, 36.7, 39.9, 51.2, 54.6, 104.3, 111.0, 113.1, 115.4, 128.1, 129.3, 129.4, 134.3, 146.2, 147.5, 158.0. HR-MS *m/z* calcd for $C_{26}H_{34}N_4O_2$ $[(M + H)]^+$: 435.2755; found 435.2766.

4.41. Methyl 4-(4-nitrophenoxy)benzoate (s)

Intermediate **s** was obtained from 4-nitrophenol and methyl 4-(bromomethyl)benzoate following the general procedure F. FC in hexane/ethyl acetate 9/1, R*f*: 0.47. Yellowish powder (71 % yield). ^{1}H NMR (400 MHz, $CDCl_3$): *δ*: 3.94 (s, 3H, C*H*$_3$); 5.12 (s, 2H, C*H*$_2$); 7.02 (d, 2H, aryl, *J* = 8.4 Hz); 7.33 (d, 2H, aryl, *J* = 8.4 Hz); 7.84 (d, 2H, aryl, *J* = 8.3 Hz); 8.16 (d, 2H, aryl, *J* = 8.3 Hz). HR-MS *m/z* calcd for $C_{14}H_{11}NO_5$.

4.42. Methyl 4-(4-aminophenoxy)benzoate (t)

Obtained from **s** applying the general procedure A. Yellowish powder (98 % yield). ^{1}H NMR (400 MHz, CD_3OD): *δ*: 3.90 (s, 3H, C*H*$_3$); 5.03 (s, 2H, C*H*$_2$); 6.71 (d, 2H, aryl, *J* = 8.8 Hz); 7.13 (d, 2H, aryl, *J* = 8.8 Hz). 7.21 (d, 2H, aryl, *J* = 8.4 Hz); 7.33 (d, 2H, aryl, *J* = 8.3 Hz); HR-MS *m/z* calcd for $C_{14}H_{13}NO_3$ $[(M + H)]^+$: 244.0968; 244.0992.

4.43. Methyl 4-(4-(3-(((3r,5r,7r)-adamantan-1-yl)methyl)ureido)phenoxy)benzoate (u)

Synthesized from **t** and 1-adamantanemethylamine following the general procedure B. FC in n-hexane/ethyl acetate 1/1, R*f*: 0.45. Yellowish powder (46 % yield). ^{1}H NMR (400 MHz, $CDCl_3$): *δ*: 1.47 (s, 6H, C*H*$_2$); 1.64 (d, 3H, C*H* and C*H*$_2$, *J* = 11.8 Hz); 1.73 (d, 3H, C*H* and C*H*$_2$, *J* = 12.1 Hz); 1.98 (bs, 3H, C*H* and C*H*$_2$); 2.95 (s, 2H, C*H*$_2$); 3.95 (s, 3H, C*H*$_3$); 4.71 (bs, 1H, N*H*); 5.13 (s, 2H, C*H*$_2$); 6.21 (bs, 1H, N*H*); 6.96 (d, 2H, aryl, *J* = 8.4 Hz); 7.23 (d, 2H, aryl, *J* = 8.4 Hz); 7.51 (d, 2H, aryl, *J* = 8.3 Hz); 8.07 (d, 2H, aryl, *J* = 8.2 Hz). HR-MS *m/z* calcd for $C_{26}H_{30}N_2O_4$ $[(M + H)]^+$: 435.2278; found 435.2233.

4.44. 4-((4-(3-(adamantan-1-ylmethyl)ureido)phenoxy)methyl)benzoic acid [15]

Final derivative **15** was obtained from **u** following the general procedure C. Precipitated from MeOH/diethyl ether. Whitish powder (92 % yield). ^{1}H NMR (400 MHz, DMSO): *δ*: 1.44 (s, 6H, C*H*$_2$); 1.59 (d, 3H, C*H* and C*H*$_2$, *J* = 11.8 Hz); 1.67 (d, 3H, C*H* and C*H*$_2$, *J* = 12.1 Hz); 1.94 (bs, 3H, C*H* and C*H*$_2$); 2.78 (d, 2H, C*H*$_2$, *J* = 6.0 Hz); 6.05 (t, 1H, N*H*); 6.90

(d, 2H, aryl, $J = 9.0$ Hz); 7.29 (d, 2H, aryl, $J = 9.0$ Hz); 7.54 (d, 2H, aryl, $J = 8.2$ Hz); 7.95 (d, 2H, aryl, $J = 8.2$ Hz); 8.24 (s, 1H, N*H*). ^{13}C NMR (100 MHz, CD_3OD) δ: 28.2, 37.1, 51.2, 69.3, 115.5, 119.4, 127.3, 129.9, 130.7, 134.7, 142.9, 153.0, 156.1, 167.7. HR-MS *m/z* calcd for $C_{26}H_{30}N_2O_4$ $[(M + Na)]^+$: 457.2103; found 457.2076.

4.45. 1-(((1s,3s)-adamantan-1-yl)methyl)-3-(4-aminobenzyl)urea (v)

Obtained from 4-aminobenzylamine and 1-adamantanemethylamine following the general procedure B. FC in n-hexane/ethyl acetate 1/1, R*f*: 0.47. Yellowish powder (45 % yield). ^{1}H NMR (400 MHz, CD_3OD): δ: 1.51 (s, 6H, CH_2); 1.68 (d, 3H, C*H* and CH_2, $J = 11.8$ Hz); 1.76 (d, 3H, C*H* and CH_2, $J = 12.0$ Hz); 1.97 (bs, 3H, C*H* and CH_2); 2.84 (s, 2H, CH_2); 4.18 (s, 2H, CH_2); 6.70 (d, 2H, aryl, $J = 8.4$ Hz); 7.06 (d, 2H, aryl, $J = 8.3$ Hz). HR-MS *m/z* calcd for $C_{19}H_{27}N_3O$ $[(M + Na)]^+$: 314.2227; found 314.2258.

4.46. Methyl 4-(((4-((3-(((1s,3s)-adamantan-1-yl)methyl)ureido)methyl)phenyl)amino)methyl)benzoate (w)

Synthesized from **v** and methyl 4-formyl benzoate following the general procedure E. FC in dichloromethane/ethyl acetate 9/1, R*f*: 0.45. Yellowish powder (57 % yield). ^{1}H NMR (400 MHz, CD_3OD): δ: 1.48 (s, 6H, CH_2); 1.68 (d, 3H, C*H* and CH_2, $J = 11.9$ Hz); 1.75 (d, 3H, C*H* and CH_2, $J = 12.1$ Hz); 1.94 (bs, 3H, C*H* and CH_2); 2.82 (s, 2H, CH_2); 3.90 (s, 2H, CH_3); 4.15 (s, 2H, CH_2); 4.40 (s, 2H, CH_2); 6.57 (d, 2H, aryl, $J = 8.4$ Hz); 7.03 (d, 2H, aryl, $J = 8.4$ Hz); 7.47 (d, 2H, aryl, $J = 8.2$ Hz); 7.96 (d, 2H, aryl, $J = 8.2$ Hz). HR-MS *m/z* calcd for $C_{28}H_{35}N_3O_3$ $[(M + Na)]^+$: 462.2751; found 462.2788.

4.47. 4-(((4-((3-(adamantan-1-ylmethyl)ureido)methyl)phenyl)amino)methyl)benzoic acid [16]

Final derivative **16** was obtained from **w** applying the general procedure C. Precipitated from MeOH/diethyl ether. Whitish powder (92 % yield). ^{1}H NMR (400 MHz, CD_3OD): δ: 1.48 (s, 6H, CH_2); 1.65 (d, 3H, C*H* and CH_2, $J = 11.9$ Hz); 1.75 (d, 3H, C*H* and CH_2, $J = 11.8$ Hz); 1.95 (bs, 3H, C*H* and CH_2); 2.82 (s, 2H, CH_2); 4.15 (s, 2H, CH_2); 4.40 (s, 2H, CH_2); 6.59 (d, 2H, aryl, $J = 7.1$ Hz); 7.04 (d, 2H, aryl, $J = 8.4$ Hz); 7.45 (d, 2H, aryl, $J = 8.0$ Hz); 7.96 (d, 2H, aryl, $J = 8.1$ Hz). ^{13}C NMR (100 MHz, CD_3OD) δ: 28.4, 36.7, 39.8, 43.2, 47.1, 51.4, 112.7, 126.7, 127.9, 127.95, 129.4, 145.7, 147.6, 160.1, 169.1. HR-MS *m/z* calcd for $C_{27}H_{33}N_3O_3$ $[(M + H)]^+$: 448.2595; found 448.2590.

4.48. Computational details

The structures of small molecules were constructed by Build Panel of Maestro (v. 11) and refined through: OPLS3 force field [42,43], the Polak–Ribier conjugate gradient algorithm (PRCG, 9×10^7 steps, maximum derivative less than 0.001 kcal/mol), in H_2O with GB/SA (generalized Born/surface area) solvent treatment [44]. The so obtained structures were processed by LigPrep [45]: checking possible tautomers and protonation state at pH of 7.0 ± 1.0. The experimental structures of sEH (PDB ID: 3I28) [37], FLAP (PDB ID: 6VGC) [34] and 5-LOX (PDB ID: 3O8Y) [46] were prepared for docking calculation by Protein Preparation Wizard [47,48]: deletion of water molecules, buffer ions and ligand; bond order assignment and all hydrogens addition; check of missing side chains, loops and residue alternate positions; assignment of the side chain protonation state considering the pK_a at physiological pH.

The molecular docking predictions of the compounds against sEH and FLAP were carried out by Glide software [49,50]. The molecular docking parameters used for sEH were previously described [21]. The receptor grid for FLAP was generated using inner and outer boxes respectively of 10 Å and 15 Å placed at the following x, y, and z coordinates: 9.32, −11.40, −15.45. The theoretical methodology was validated by docking the co-crystallized ligand DG-031 with FLAP and then the docked and experimental conformations were superimposed, obtaining an RMSD = 0.875 Å [51–53]. Specifically, one pose per ligand was obtained by Standard Precision (SP) with default parameters. The SP prediction docked poses were used as input conformations for three rounds of Extra Precision (XP) mode calculations with default parameters but adding: ring conformation sampling also of the input geometry and filtering only amide bond trans conformation. The enhanced sampling mode was utilized, filtering 10,000 poses/ligand for the initial docking step, 1000 poses/ligand for energy minimization and 1600 maximum output structures/ligand. Post-docking optimization was performed on docked conformations, sorting 100 maximum number of poses. Epik state penalty, aromatic bonds and intramolecular H-bond reward, were accounted as energy contributions. The extended protocol of the Induced Fit Docking [48,54,55], with XP precision mode and defaults parameters, was employed for screening the small molecules *vs.* 5-LOX, producing 80 ligand–protein poses. Two rounds of calculations were performed using the top-ranked conformation of each ligand from the first round as input geometry for the second run. The grid with a 10 Å inner box was centred on Fe^{2+} while the outer box was automatically yielded. Maestro (version 11) was employed for docking outcome analysis and figure preparation.

4.49. In vitro pharmacological characterization

4.49.1. Cell-free 5-LOX activity assay

Human recombinant 5-LOX was expressed in *E. coli* Bl21 (DE3) cells, transformed with the plasmid pT3–5LO and 5-LOX was isolated using an ATP-agarose column by affinity chromatography [56]. *E. coli* were lysed in 50 mM triethanolamine/HCl pH 8.0 with EDTA (5 mM), soybean trypsin inhibitor (60 μg/mL), phenylmethanesulfonyl fluoride (1 mM), dithiothreitol (1 mM), and lysozyme (1 mg/mL) and sonified 3 times for 15 s. The homogenate was centrifuged at 40,000×*g* for 20 min at 4 °C and the supernatant was transferred to an ATP-agarose column (Sigma-Aldrich, Deisenhofen, Germany), which was sequentially washed with PBS pH 7.4, 1 mM EDTA, 50 mM phosphate buffer pH 7.4, 0.5 M NaCl, 1 mM EDTA, and finally 50 mM phosphate buffer pH 7.4 plus 1 mM EDTA. The enzyme was eluted with 50 mM phosphate buffer pH 7.4, 1 mM EDTA, and 20 mM ATP.

Isolated 5-LOX (0.5 μg in PBS pH 7.4 containing 1 mM EDTA) was pre-incubated with vehicle (DMSO) or test compounds for 15 min on ice. 5-LOX product formation was started by addition of 20 μM arachidonic acid (Sigma-Aldrich) and $CaCl_2$ (2 mM) and stopped by addition of an equal volume of ice-cold methanol containing PGB_1 (200 ng) as internal standard after 10 min at 37 °C. Major 5-LOX products (all-*trans* isomers of LTB_4 and 5-HETE) were extracted on Sep-Pak C18 35 cc Vac Cartridges (Waters, Milford, MA), separated by RP-HPLC on a Nova-Pak C18 Radial-Pak Column (4 μm, 5 × 100 mm, Waters) under isocratic conditions (73 % methanol/27 % water/0.007 % trifluoroacetic acid) at a flow rate of 1.2 mL/min and detected at 235 and 280 nm [56].

4.49.2. Activity assays of isolated COX-1 and COX-2

Purified ovine COX-1 (Cayman Chemicals; 50 units) or human recombinant COX-2 (Cayman Chemicals; 20 units) were diluted in 100 mM Tris buffer pH 8, containing 5 mM glutathione, 5 μM hemoglobin, and 100 μM EDTA. Samples were pre-incubated with test compounds or vehicle (0.1 % DMSO) for 5 min at 4 °C, followed by 1 min at 37 °C. Then, AA (5 μM for COX-1 and 2 μM for COX-2) was added, and incubations were continued for another 10 min at 37 °C. Formation of COX-derived 12-hydroxyheptadecatrienoic acid (12-HHT) from AA was analyzed by RP-HPLC as described previously [57].

4.49.3. Preparation of mPGES-1 in microsomes of A549 cells and determination of PGE_2 formation

Preparation of A549 cells and determination of mPGES-1 activity under cell-free assay conditions was performed as described previously [58]. In brief, cells were treated with 1 ng mL^{-1} interleukin-1β for 48 h

at 37 °C and 5 % CO_2, followed by sonification. The homogenate was subjected to differential centrifugation at 10,000 g for 10 min and 174,000 g for 1 h at 4 °C. The pellet (microsomal fraction) was resuspended in 1 mL of homogenization buffer (0.1 M potassium phosphate buffer, pH 7.4, 1 mM phenylmethanesulfonyl fluoride, 60 μg/mL soybean trypsin inhibitor, 1 μg/mL leupeptin, 2.5 mM glutathione, and 250 mM saccharose), and the total protein concentration was determined using Bradford protein assay. Microsomal membranes were diluted in potassium phosphate buffer (0.1 M, pH 7.4) containing 2.5 mM glutathione. Test compounds or vehicle were added, and after 15 min at 4 °C, the reaction (100 μL total volume) was initiated by addition of 20 μM PGH_2 (final concentration). After 1 min at 4 °C, the reaction was terminated using stop solution (100 μL; 40 mM $FeCl_2$, 80 mM citric acid, and 10 μM 11β-PGE_2 as internal standard). Then, PGH_2 was added and all samples were incubated for 1 min at 4 °C. Formed PGE_2 was separated by solid-phase extraction and analyzed by RP-HPLC [58].

4.49.4. Analysis of cell-free sEH activity

Human recombinant sEH was expressed in Sf9 insect cells and isolated by affinity chromatography. In brief, Sf9 cells were infected with a recombinant baculovirus and lysed after 72 h in 50 mM $NaHPO_4$ pH 8, 300 mM NaCl, 10 % glycerol, 1 mM EDTA, 1 mM phenylmethanesulfonyl fluoride, 10 μg/mL leupeptin, and 60 μg/mL STI by sonication (3 × 10 s, 4 °C). Sequential centrifugation at 20,000g (10 min, 4 °C) and 100,000g (60 min, 4 °C) yielded a supernatant, which was then subjected to benzylthio-sepharose affinity chromatography. Elution with 4-fluorochalcone oxide in PBS pH 7.4 with 1 mM dithiothreitol and 1 mM EDTA yielded sEH, which was dialyzed and concentrated. Isolated sEH (60 ng) in 25 mM Tris HCl pH 7 with 0.1 mg/mL bovine serum albumin (BSA) was preincubated with the vehicle (DMSO) or test compounds for 1 min at room temperature. The sEH substrate PHOME (20 μM, Cayman Chemicals) was added to start the enzymatic reaction, which was stopped after 60 min in the darkness by addition of $ZnSO_4$ (200 mM). The formation of the fluorescent product 6-methoxy-naphtaldehyde was measured using a NOVOstar fluorescence microplate reader (BMG Labtech, Ortenberg, Germany), with excitation at 330 and emission at 465 nm.

4.49.5. Human cells

Monocytes and neutrophils were isolated from leukocyte concentrates obtained from freshly withdrawn peripheral blood of healthy adult male and female donors, provided by the Institute of Transfusion Medicine, University Hospital Jena, Germany. The experimental protocol was approved by the ethical committee of the University Hospital Jena (approval no. 5050–01/17). All methods were performed in accordance with the relevant guidelines and regulations. This protocol is described in detail in Günther et al. [59] In brief, leukocyte concentrates were mixed with dextran (derived from *Leuconostoc* spp. MW ~40,000, Sigma Aldrich) for sedimentation of erythrocytes. The supernatant was centrifuged on lymphocyte separation medium (Histopaque®-1077, Sigma Aldrich). Contaminating erythrocytes in the pelleted neutrophil fraction were removed by hypotonic lysis using distilled water. Neutrophils were then washed twice in ice-cold PBS pH 7.4 and finally resuspended in PBS pH 7.4 plus 1 mg/mL glucose (PG buffer). The peripheral blood mononuclear cell (PBMC) fraction was seeded in RPMI 1640 (Sigma-Aldrich) containing 10 % (v/v) heat-inactivated fetal calf serum (FCS), 100 U/mL penicillin, and 100 μg/mL streptomycin in cell culture flasks (Greiner Bio-one, Frickenhausen, Germany) and incubated for 1.5 h at 37 °C and 5 % CO_2 for adherence of monocytes. For differentiation of monocytes to macrophages and subsequent polarization towards M1-and M2-MDM, we used published criteria and procedures [59,60]. Thus, M1-MDM were generated by incubating monocytes with 20 ng/mL GM-CSF (Peprotech, Hamburg, Germany) for 6 days in RPMI 1640 supplemented with 10 % FCS, 2 mmol/L L-glutamine (Biochrom/Merck, Berlin, Germany), 100 U/mL penicillin, and 100 μg/mL streptomycin, followed by treatment with 100 ng mL^{-1} lipopolysaccharide and 20 ng mL^{-1} interferon-γ (Peprotech) for another 24 h. M2-MDM were obtained by incubating monocytes with 20 ng/mL M-CSF (Peprotech) for 6 days and subsequent polarization by treatment with 20 ng mL^{-1} interleukin (IL)-4 (Peprotech) for 48 h.

4.49.6. 5-LOX product formation in human neutrophils

Freshly isolated neutrophils (5×10^6) suspended in PBS pH 7.4 with 1 mg/mL glucose were preincubated with the test compounds for 15 min on ice. 5-LOX product formation in neutrophils was evoked by addition of Ca^{2+}-ionophore A23187 (2.5 μM, Sigma-Aldrich) with or without 20 μM AA (as indicated) followed by incubation for 10 min at 37 °C. The reaction was stopped with an equal volume of methanol containing PGB_1 (200 ng) as internal standard. Major 5-LOX products (all-trans isomers of LTB and 5-HETE, and additionally LTB_4) were extracted and analyzed by RP-HPLC as described for the determination of cell-free 5-LOX activity.

4.49.7. Analysis of lipid mediator profiles of macrophages by UPLC-MS/MS

Polarized M1-and M2-MDM (at the indicated numbers) were incubated in PBS plus 1 mM $CaCl_2$. To determine the potential of compound **6** to initiate the LM class switch, M1-/M2-MDM were first treated with indicated concentrations of compound **6** for 30 min and then stimulated with SACM (1 %) at 37 °C for 90 min. SACM was produced as previously described [39]. After the indicated incubation periods, the supernatants (1 mL) were transferred to 2 mL of ice-cold methanol containing deuterium-labeled internal standards (200 nM d8-5S-HETE, d4-LTB_4, d5-LTC_4, d5-LTD_4, d5-LTE_4, d5-LXA_4, d5-RvD2 and d4-PGE_2 Cayman Chemical/Biomol GmbH, Hamburg, Germany) to facilitate quantification and sample recovery. Solid phase extraction (SPE) and sample preparation for UPLC-MS/MS analysis was conducted by adapting published criteria [61]. Briefly, samples were kept at −20 °C for 60 min to allow protein precipitation. After centrifugation (1200×*g*, 4 °C, 10 min), 9 mL acidified H_2O was added to the supernatants (pH = 3.5) and samples were subjected to SPE. Solid phase cartridges (Sep-Pak® Vac 6 cc 500 mg/6 mL C18; Waters, Milford, MA) were equilibrated with 6 mL methanol and 2 mL H_2O. Then, samples were loaded onto columns and washed with 6 mL H_2O and additional 6 mL *n*-hexane. Non-cysteinylated-LM were eluted with 6 mL methyl formate in glass vials, and then cysteinylated-LM (LTC_4, LTD_4 and LTE_4) were eluted with 6 mL methanol into separate glass vials. The eluates were brought to dryness using an evaporation system (TurboVap LV, Biotage, Uppsala, Sweden), and LM were resuspended in 100 μL methanol/water (50:50, v/v) for UPLC-MS/MS analysis. LM profile was analyzed with a with a Nexera X2 UHPLC system (Shimadzu Corporation, Kyoto, Japan) coupled with a QTrap 7500 mass spectrometer, controlled by SCIEX-OS (SCIEX, Framingham, MA, USA). LM were separated using an ACQUITY UPLC® BEH C18 column (1.7 μm, 2.1 × 100 mm; Waters, Eschborn, Germany) at 50 °C with a flow rate of 0.3 mL/min and a mobile phase consisting of methanol/water/formic acid of 42.0/57.9/0.1 (v/v/v) that was ramped to 80.7/19.2/0.1 (v/v/v) over 11 min and then to 97.9/2/0.1 (v/v/v) for 5 min. QTrap 7500 mass spectrometer was operated in the negative ionization mode (for non-cysteinylated LMs) and in the positive mode (for cysteinylated LMs) using scheduled multiple reaction monitoring coupled with information-dependent acquisition (Table S1). The scheduled multiple reaction monitoring window was 60 s, optimized MS/MS parameters in the negative (Table S2) and positive ionization mode (Table S3) were used as given in the tables below. The retention time and diagnostic ions for each oxylipin were confirmed using an external commercially available standard (Cayman Chemical, Ann Arbor, MI, US). Quantification was achieved by linear calibration curves for each lipid mediator. Only peaks with a minimum signal-to-noise ratio of 10 were quantified.

4.49.8. Zymosan-induced peritonitis

CD-1 mice (33–39 g, 8 weeks old; Charles River Laboratories, Calco,

Italy) were housed under standard conditions with free access to standard rodent chow and water. Animals were acclimatized for 4 days under a 12 h light/12 h dark cycle in a temperature-controlled environment (21 ± 2 °C). Mice were randomly assigned to experimental groups, and all procedures were conducted during the light phase. All animal experiments were performed in accordance with Italian (D.L. 26/2014) and European (Directive 2010/63/EU) legislation on the protection of animals used for scientific purposes and were approved by the Italian Ministry of Health. Mice were pre-treated intraperitoneally with compound **6** (10 mg/kg) or vehicle (0.5 mL, DMSO 2 % in PBS Tween 20 3 % and PEG 400 3 %; ZYM group) 30 min prior to intraperitoneal injection of zymosan (2 mg/mL in saline, 0.5 mL; Sigma-Aldrich). Mice were sacrificed by CO_2 inhalation 4 h after zymosan administration for subsequent analysis of LM by LC-MS/MS.

4.50. LM analysis in vivo samples

4.50.1. Extraction of LMs from exudate samples

The extraction of LMs from exudates was performed as follows: 500 μL of exudate from each sample were spiked with a mix of deuterated standards and subsequently diluted with 500 μL of phosphate-buffered saline (PBS), details for both authentic and deuterium labeled standards are reported in Table S4. Samples were then loaded on solid-phase extraction cartridges, Strata-X Polymeric reversed-phase SPE columns (100 mg/3 mL) (Phenomenex, Bologna, Italy). Cartridges were conditioned with 3 mL of MeOH and equilibrated with 3 mL of ddH_2O. Following loading, columns were washed with 1 mL of 10 % MeOH *v/v*, and LMs were finally eluted with 1.5 mL of MeOH. Eluted samples were dried with a SpeedVac (Savant, Thermo Scientific, Milan, Italy) and dissolved prior to UHPLC-MS/MS analyses in 50 μL of methanol LC-MS Grade.

4.50.2. UPLC-MS/MS analysis of LMs profile in vivo

UPLC-MS/MS analyses were acquired using an ACQUITY UPLC I-Class PLUS (Waters, Milford, MA, USA), coupled online to a triple quadrupole MS Xevo TQ-XS (Waters, Milford, MA, USA) equipped with an electrospray ionization (ESI) source operating in ESI negative mode. The separation was performed on a Kinetex® EVO C18 150 mm × 2.1 mm, 2.6 μm (100 Å) (Phenomenex, Bologna, Italy). The flow rate was set to 0.4 mL/min, and the column oven was set at 40 °C. The mobile phases were (A) H_2O/ACN (70:30) acidified with 0.02 % CH_3COOH *v/v* and (B) ACN/IPA (50:50). The following gradient was used: 0 min, 0 % B, 0–12 min 60 % B, 12.10 min, 60–99 % B, 12.10–13.05 isocratic to 99 % B; returning to 0 % B in 0.1. The injection volume was 5 μL. MS source parameters: capillary voltage 3.5 kV, desolvation gas flow and temperature were set to 1200 (L h^{-1}) and 500 °C respectively, source temperature 150 °C, sample cone gas flow 150 L/h and collision gas (argon) to 0.18 mL/min. Each analyte was optimized by direct infusion, using standard solution at 0.2 μg/mL. MRM details, such as cone voltages, dwell time, collision energies, parents and daughter ions are reported in Table S4. For the quantitative analysis LMs were used as external standards. Stock solutions (1 mg mL^{-1}) were prepared in MeOH, and the calibration curves were obtained in a concentration range of 0.1–200 ng mL^{-1} using five concentration levels with triplicate injections for each level. Linear regression was used to generate the calibration curves with R^2 values ≥ 0.999. Extracted ion chromatograms (XIC) area of the standard were plotted against corresponding concentrations (ng mL^{-1}). The samples analyses were performed randomly on three technical replicates and the quantification of analytes was evaluated in terms of an average, showed as pM ± Standard Error of the Mean (S.E.M). Limits of detection (LOD) and quantification (LOQ) were calculated by using the standard deviation (SD) and the slope of the calibration curve, multiplied by 3.3 and 10, repeatability was assessed by evaluation of peak area and rt of QC samples and reported as CV% values, all results are reported in Table S5.

4.51. In vivo determination of plasma concentration of compound 6 in mice

4.51.1. Sample preparation

For the extraction of compound **6** from mouse plasma, a protein precipitation method was employed. Briefly, frozen plasma samples were thawed at room temperature. Then, 200 μL of ice-cold acetonitrile containing IS were added to 100 μL of plasma. The mixture was vortexed for 5 min and subsequently centrifuged at 14,000 rpm for 10 min at 4 °C. The resulting supernatants were collected and analyzed by LC-MS/MS.

4.51.2. UHPLC-MS/MS conditions for compound 6 quantitation

Analyses were performed using a Nexera X3 UHPLC system (Shimadzu, Kyoto, Japan) consisting of a SCL-40 system controller, two LC-40D X3 pumps, a CTO-40C column oven and, a SIL-40C X3 autosampler. The chromatographic platform was coupled online to a SCIEX Triple Quad™ 7500 LC-MS/MS system equipped with an OptiFlow™ ionization source (SCIEX, Framingham, Massachusetts, USA).

The chromatographic separation was performed on a Kinetex® 2.6 μm EVO C18 100 Å, LC Column 50 × 2.1 mm (Phenomenex, Bologna, Italy). The column temperature and the flow rate were set at 40 °C and 0.4 mL/min, respectively. The mobile phases were: H_2O (A) and ACN (B) both acidified with 0.1 % HCOOH (*v/v*) with the following gradient: 0.00–5.00 min, 5–95 % B; 5.01–6.00 min, isocratic to 95 % B; 6.01–6.50 min, 95-5 % B; then 1 min and half for column re-equilibration.

MS data were acquired in positive ionization mode with a curtain gas flow rate of 40 psi, gas 1 flow rate of 60 psi, gas 2 flow rate of 55 psi, an interface voltage of 4800 V, and an interface temperature of 400 °C. Multiple Reaction Monitoring (MRM) parameters are reported in Table S3.

4.51.3. Preparation of stock, working, calibration and quality control standard solutions

Stock solutions of compound **6** and the internal standard (IS) were prepared in DMSO at a concentration of 1 μg/mL. Working standard solutions were prepared by diluting the compound **6** stock solution with acetonitrile.

Calibration standards were prepared by diluting the corresponding standard working solutions with blank mouse plasma to obtain final concentrations of 1.00, 2.50, 5.00, 10.0, 25.0, 50.0 and, 100.0 ng mL^{-1}. An equal amount of IS was added for each level to achieve a final concentration of 4 ng mL^{-1}.

Quality control (QC) samples with concentrations of 1.00 ng mL^{-1} (lower limit of quantification, LLOQ), 5.00 ng mL^{-1} (LQC, low-quality control), 50.0 ng mL^{-1} (MQC, medium-quality control) and 100.0 ng mL^{-1} (HQC, high-quality control) were prepared in a similar manner. The LLOQ was determined based on a signal-to-noise (S/N) ratio of at least 10.

The calibration curve was constructed by plotting the ratio of the peak areas of **6**/IS (y) against the nominal concentration of **6** (x) in the form of $y = ax + b$, and the least squares method was used for the linear regression analysis with R^2 values ≥ 0.999.

4.51.4. Precision and accuracy

Method precision was expressed as the relative standard deviation (RSD) of replicate measurements, while accuracy was evaluated as the ratio between the calculated and theoretical concentrations. Intra-day accuracy and precision of the UHPLC-MS/MS method were assessed by analyzing QC samples (5.00 ng mL^{-1}, 50.0 ng mL^{-1}, and 100.0 ng mL^{-1}) and LLOQ samples (1.00 ng mL^{-1}), using three replicates per concentration on the same day. Inter-day accuracy and precision were evaluated by analyzing QC samples over three consecutive days.

According to the FDA guidelines [U.S. Food and Drug Administration, Bioanalytical Method Validation. Guidance for Industry, 2018], the criterion for precision and accuracy was that the RSD should be ≤ 15 % for each concentration except the LLOQ (≤20 %).

The intraday accuracy for **6** ranged from 99.17 to 105.23 %, and the inter-day accuracy ranged from 99.65 to 106.33 %. The intra- and inter-day precisions were 1.39–3.76 % and 0.87–2.59 %, respectively. The results showed that this method was accurate, reliable and reproducible (Table S4).

4.51.5. Statistical analysis

The results are expressed as mean ± S.E.M of the mean of n observations, where n represents the number of animals or number of experiments performed at different days. Statistical evaluation was performed by one–way ANOVA using GraphPad Prism 10 (Graphpad Software Inc., San Diego, CA) followed by Tukey's or Dunnett's post hoc tests for multiple comparisons, respectively. Post hoc tests were run only when F achieved $P < 0.05$ and there was no significant variance in the homogeneity. A P value < 0.05 was used to define statistically significant differences between mean values.

CRediT authorship contribution statement

Tania Ciaglia: Investigation. **Danilo D'Avino:** Investigation. **Paul M. Jordan:** Investigation. **Simone Di Micco:** Investigation. **Simona Musella:** Formal analysis. **Hannes Engelbrecht:** Investigation. **Lukas Klaus Peltner:** Investigation, Formal analysis. **Veronica Di Sarno:** Formal analysis, Data curation. **Fabrizio Merciai:** Investigation. **Sara Perna:** Investigation. **Gerardina Smaldone:** Formal analysis, Data curation. **Francesca Di Matteo:** Validation, Formal analysis. **Valeria Napolitano:** Methodology. **Rosario Stimoli:** Methodology. **Giuseppe Bifulco:** Writing – original draft, Validation. **Giacomo Pepe:** Supervision, Data curation. **Eduardo Maria Sommella:** Formal analysis, Conceptualization. **Manuela Giovanna Basilicata:** Validation, Methodology. **Giovanna Aquino:** Methodology, Data curation. **Isabel M. Gomez-Monterrey:** Writing – original draft, Project administration. **Pietro Campiglia:** Writing – original draft, Supervision. **Carmine Ostacolo:** Writing – review & editing, Validation. **Oliver Werz:** Writing – review & editing, Validation, Conceptualization. **Antonietta Rossi:** Writing – review & editing, Writing – original draft, Conceptualization. **Alessia Bertamino:** Writing – original draft, Supervision, Methodology, Conceptualization. **Michele Manfra:** Project administration, Methodology, Funding acquisition.

Declaration of competing interest

The authors declare that they have no known competing financial interests or personal relationships that could have appeared to influence the work reported in this paper.

Acknowledgements

This research was supported in part by the project: New approach in the treatment of inflammation: development of 5-LOX/sEH dual inhibitors and their pharmacological characterization (NAIDI), MIUR CODE: P2022CNPH8, CUP: C53D23007850001 to AR and MM and project - Digital Driven Diagnostics, prognostics and therapeutics for sustainable Health care (D34H) "CUP" B53C22006090001 to PC.; DD was the recipient of a research grant from "Progetto di Eccellenza 2022–2027 TRAVEL, Department of Pharmacy, University of Naples Federico II"; This work was funded by PNRR – Missione 4 "Istruzione e Ricerca" Componente 2 "Dalla Ricerca all'Impresa" – Investimento 1.2. "Finanziamento di progetti presentati da giovani ricercatori" –research project: "Sviluppo di inibitori duali della 5-lipossigenasi (5-LOX) e della epossido idrolasi solubile (sEH), dotati di un profilo farmacocinetico e farmacodinamico in grado di superare i limiti dell'hit compound", CUP D47G25000090006 to TC. This work was supported by the Deutsche Forschungsgemeinschaft, SFB 1127/3 ChemBioSys 239748522 project A04 and SFB1278/2 Polytarget 316213987 project A04 and C02 (to O. W.). We thank the Free State of Thuringia/Thüringer Aufbaubank and the European Union/Europäischer Fonds für regionale Entwicklung (2023 FGI 0012) for financial support.

Appendix A. Supplementary data

Supplementary data to this article can be found online at https://doi.org/10.1016/j.ejmech.2025.118338.

Data availability

Data will be made available on request.

References

[1] C.N. Serhan, N.A. Petasis, Resolvins and protectins in inflammation resolution, Chem Rev 111 (10) (2011) 5922–5943, https://doi.org/10.1021/cr100396c.
[2] B. Wang, L. Wu, J. Chen, L. Dong, C. Chen, Z. Wen, J. Hu, I. Fleming, D.W. Wang, Metabolism pathways of arachidonic acids: mechanisms and potential therapeutic targets, Signal Transduct Target Ther 6 (1) (2021), https://doi.org/10.1038/s41392-020-00443-w.
[3] B. Díez-Dacal, D. Pérez-Sala, Anti-inflammatory prostanoids: focus on the interactions between electrophile signaling and resolution of inflammation, Sci. World J. 10 (2010) 655–675, https://doi.org/10.1100/tsw.2010.69.
[4] V.L. Ott, J.C. Cambier, J. Kappler, P. Marrack, B.J. Swanson, Mast cell–dependent migration of effector CD8+ T cells through production of leukotriene B4, Nat. Immunol. 4 (10) (2003) 974–981, https://doi.org/10.1038/ni971.
[5] J. Bjrk, P. Hedqvist, K.-E. Arfors, Increase in vascular permeability induced by leukotriene b4 and the role of polymorphonuclear leukocytes, Inflammation 6 (2) (1982) 189–200, https://doi.org/10.1007/bf00916243.
[6] J. Harwood, E. Lloyd-Evans, N. Chiang, Charles N. Serhan, Specialized pro-resolving mediator network: an update on production and actions, Essays Biochem. 64 (3) (2020) 443–462, https://doi.org/10.1042/ebc20200018.
[7] M. Mainka, S. George, C. Angioni, R. Ebert, T. Goebel, N. Kampschulte, A. Krommes, A. Weigert, D. Thomas, N.H. Schebb, et al., On the biosynthesis of specialized pro-resolving mediators in human neutrophils and the influence of cell integrity, BBA-MOL CELL BIOL L 1867 (3) (2022), https://doi.org/10.1016/j.bbalip.2021.159093.
[8] C. Kretzer, P.M. Jordan, R. Bilancia, A. Rossi, T. Gür Maz, E. Banoglu, U. S. Schubert, O. Werz, Shifting the biosynthesis of leukotrienes toward specialized pro-resolving mediators by the 5-Lipoxygenase-Activating protein (FLAP) antagonist BRP-201, J. Inflamm. Res. 15 (2022) 911–925, https://doi.org/10.2147/jir.S345510.
[9] T.R. Harris, B.D. Hammock, Soluble epoxide hydrolase: gene structure, expression and deletion, Gene 526 (2) (2013) 61–74, https://doi.org/10.1016/j.gene.2013.05.008.
[10] A.A. Spector, A.W. Norris, Action of epoxyeicosatrienoic acids on cellular function, American Am J Physiol Cell Physiol 292 (3) (2007) C996–C1012, https://doi.org/10.1152/ajpcell.00402.2006.
[11] A.A. Spector, X. Fang, G.D. Snyder, N.L. Weintraub, Epoxyeicosatrienoic acids (EETs): metabolism and biochemical function, Prog. Lipid Res. 43 (1) (2004) 55–90, https://doi.org/10.1016/s0163-7827(03)00049-3.
[12] K.R. Schmelzer, L. Kubala, J.W. Newman, I.-H. Kim, J.P. Eiserich, B.D. Hammock, Soluble epoxide hydrolase is a therapeutic target for acute inflammation, Proc. Natl. Acad. Sci. USA 102 (28) (2005) 9772–9777, https://doi.org/10.1073/pnas.0503279102.
[13] W. Zhang, A.L. Yang, J. Liao, H. Li, H. Dong, Y.T. Chung, H. Bai, K.A. Matkowskyj, B.D. Hammock, G.-Y. Yang, Soluble epoxide hydrolase gene deficiency or inhibition attenuates chronic active inflammatory bowel disease in IL-10(−/−) mice, Dig. Dis. Sci. 57 (10) (2012) 2580–2591, https://doi.org/10.1007/s10620-012-2217-1.
[14] E. Ikdahl, A. Kerola, E. Sollerud, A.G. Semb, Cardiovascular implications of non-steroidal anti-inflammatory drugs: a comprehensive review, with emphasis on patients with rheumatoid arthritis, ECR (Exp. Cell Res.) 19 (2024), https://doi.org/10.15420/ecr.2024.24.
[15] H.E. Vonkeman, M.A.F.J. van de Laar, Nonsteroidal anti-inflammatory drugs: adverse effects and their prevention, Semin. Arthritis Rheum. 39 (4) (2010) 294–312, https://doi.org/10.1016/j.semarthrit.2008.08.001.
[16] Vascular and upper gastrointestinal effects of non-steroidal anti-inflammatory drugs: meta-analyses of individual participant data from randomised trials, Lancet 382 (9894) (2013) 769–779, https://doi.org/10.1016/s0140-6736(13)60900-9.
[17] X. Huo, Y. Gu, Y. Zhang, The discovery of multi-target compounds with anti-inflammation activity from traditional Chinese medicine by TCM-target effects relationship spectrum, J. Ethnopharmacol. 293 (2022), https://doi.org/10.1016/j.jep.2022.115289.
[18] P.A. Elzahhar, R. Alaaeddine, T.M. Ibrahim, R. Nassra, A. Ismail, B.S.K. Chua, R. L. Frkic, J.B. Bruning, N. Wallner, T. Knape, et al., Shooting three inflammatory targets with a single bullet: novel multi-targeting anti-inflammatory glitazones, Eur. J. Med. Chem. 167 (2019) 562–582, https://doi.org/10.1016/j.ejmech.2019.02.034.
[19] W.A. Badawi, M. Rashed, A. Nocentini, A. Bonardi, M.M. Abd-Alhaseeb, S.T. Al-Rashood, G.B. Veerakanellore, T.A. Majrashi, E.B. Elkaeed, B. Elgendy, et al., Identification of new 4-(6-oxopyridazin-1-yl)benzenesulfonamides as multi-target

anti-inflammatory agents targeting carbonic anhydrase, COX-2 and 5-LOX enzymes: synthesis, biological evaluations and modelling insights, J Enzyme Inhib Med Chem 38 (1) (2023), https://doi.org/10.1080/14756366.2023.2201407.
[20] I. Cerqua, S. Musella, L.K. Peltner, D. D'Avino, V. Di Sarno, E. Granato, V. Vestuto, R. Di Matteo, S. Pace, T. Ciaglia, et al., Discovery and optimization of indoline-based compounds as dual 5-LOX/sEH inhibitors: in vitro and in vivo anti-inflammatory characterization, J. Med. Chem. 65 (21) (2022) 14456–14480, https://doi.org/10.1021/acs.jmedchem.2c00817.
[21] S. Musella, D. D'Avino, L.K. Peltner, V. Di Sarno, I. Cerqua, F. Merciai, V. Vestuto, T. Ciaglia, G. Smaldone, F. Di Matteo, et al., Design, synthesis, and pharmacological characterization of a potent soluble epoxide hydrolase inhibitor for the treatment of acute pancreatitis, J. Med. Chem. 66 (13) (2023) 9201–9222, https://doi.org/10.1021/acs.jmedchem.3c00831.
[22] C. Morisseau, B.D. Hammock, Impact of soluble epoxide hydrolase and epoxyeicosanoids on human health, Annu. Rev. Pharmacol. Toxicol. 53 (1) (2013) 37–58, https://doi.org/10.1146/annurev-pharmtox-011112-140244.
[23] J. Warner, J. Hardesty, K. Zirnheld, C. McClain, D. Warner, I. Kirpich, Soluble epoxide hydrolase inhibition in liver diseases: a review of current research and knowledge gaps, Biology 9 (6) (2020), https://doi.org/10.3390/biology9060124.
[24] R.D. Jones, J. Liao, X. Tong, D. Xu, L. Sun, H. Li, G.-Y. Yang, Epoxy-oxylipins and soluble epoxide hydrolase metabolic pathway as targets for NSAID-induced gastroenteropathy and inflammation-associated carcinogenesis, Front. Pharmacol. 10 (2019), https://doi.org/10.3389/fphar.2019.00731.
[25] A.L. Lazaar, L. Yang, R.L. Boardley, N.S. Goyal, J. Robertson, S.J. Baldwin, D. E. Newby, I.B. Wilkinson, R. Tal-Singer, R.J. Mayer, et al., Pharmacokinetics, pharmacodynamics and adverse event profile of GSK2256294, a novel soluble epoxide hydrolase inhibitor, Br. J. Clin. Pharmacol. 81 (5) (2016) 971–979, https://doi.org/10.1111/bcp.12855.
[26] W.K. Schmidt, I. Cortés-Puch, C.B. McReynolds, G.E. Croston, S.H. Hwang, J. Yang, T.L. Pedersen, K.M. Wagner, T.T. Pham, T. Hunt, et al., Randomized, double-blind, phase 1a single-ascending dose and food effect studies assessing safety and pharmacokinetics of EC5026 in healthy volunteers, CTS 17 (9) (2024), https://doi.org/10.1111/cts.70033.
[27] R.P. Martini, D. Siler, J. Cetas, N.J. Alkayed, E. Allen, M.M. Treggiari, A double-blind, randomized, placebo-controlled trial of soluble epoxide hydrolase inhibition in patients with aneurysmal subarachnoid hemorrhage, Neurocrit. Care 36 (3) (2021) 905–915, https://doi.org/10.1007/s12028-021-01398-8.
[28] Z. Honetschlägerová, A. Sporková, L. Kopkan, Z. Husková, S.H. Hwang, B. D. Hammock, J.D. Imig, H.J. Kramer, P. Kujal, Z. Vernerová, et al., Inhibition of soluble epoxide hydrolase improves the impaired pressure–natriuresis relationship and attenuates the development of hypertension and hypertension-associated end-organ damage in Cyp1a1-Ren-2 transgenic rats, J. Hypertens. 29 (8) (2011) 1590–1601, https://doi.org/10.1097/HJH.0b013e328349062f.
[29] D. Chen, R. Whitcomb, E. MacIntyre, V. Tran, Z.N. Do, J. Sabry, D.V. Patel, S. K. Anandan, R. Gless, H.K. Webb, Pharmacokinetics and pharmacodynamics of AR9281, an inhibitor of soluble epoxide hydrolase, in single- and multiple-dose studies in healthy human subjects, J. Clin. Pharmacol. 52 (3) (2013) 319–328, https://doi.org/10.1177/0091270010397049.
[30] D. Pettersen, O. Davidsson, C. Whatling, Recent advances for FLAP inhibitors, Bioorg. Med. Chem. Lett. 25 (13) (2015) 2607–2612, https://doi.org/10.1016/j.bmcl.2015.04.090.
[31] Z.T. Gür, B. Çalışkan, E. Banoglu, Drug discovery approaches targeting 5-lipoxygenase-activating protein (FLAP) for inhibition of cellular leukotriene biosynthesis, Eur. J. Med. Chem. 153 (2018) 34–48, https://doi.org/10.1016/j.ejmech.2017.07.019.
[32] U. Garscha, E. Romp, S. Pace, A. Rossi, V. Temml, D. Schuster, S. König, J. Gerstmeier, S. Liening, M. Werner, et al., Pharmacological profile and efficiency in vivo of diflapolin, the first dual inhibitor of 5-lipoxygenase-activating protein and soluble epoxide hydrolase, Sci. Rep. 7 (1) (2017), https://doi.org/10.1038/s41598-017-09795-w.
[33] L. Vieider, E. Romp, V. Temml, J. Fischer, C. Kretzer, M. Schoenthaler, A. Taha, V. Hernández-Olmos, S. Sturm, D. Schuster, et al., Synthesis, biological evaluation and structure–activity relationships of diflapolin analogues as dual sEH/FLAP inhibitors, ACS Med. Chem. Lett. 10 (1) (2018) 62–66, https://doi.org/10.1021/acsmedchemlett.8b00415.
[34] J.D. Ho, M.R. Lee, C.T. Rauch, K. Aznavour, J.S. Park, J.G. Luz, S. Antonysamy, B. Condon, M. Maletic, A. Zhang, et al., Structure-based, multi-targeted drug discovery approach to eicosanoid inhibition: dual inhibitors of mPGES-1 and 5-lipoxygenase activating protein (FLAP), BBA Gen. Subj. 1865 (2) (2021), https://doi.org/10.1016/j.bbagen.2020.129800.
[35] A.D. Ferguson, B.M. McKeever, S. Xu, D. Wisniewski, D.K. Miller, T.-T. Yamin, R. H. Spencer, L. Chu, F. Ujjainwalla, B.R. Cunningham, et al., Crystal structure of inhibitor-bound human 5-Lipoxygenase-Activating protein, Science 317 (5837) (2007) 510–512, https://doi.org/10.1126/science.1144346.
[36] S. Di Micco, S. Terracciano, M. Pierri, V. Cantone, S. Liening, S. König, U. Garscha, R.K. Hofstetter, A. Koeberle, O. Werz, et al., Identification of 2,4-Dinitro-Biphenyl-Based compounds as MAPEG inhibitors, ChemMedChem 17 (22) (2022), https://doi.org/10.1002/cmdc.202200327.
[37] A.B. Eldrup, F. Soleymanzadeh, S.J. Taylor, I. Muegge, N.A. Farrow, D. Joseph, K. McKellop, C.C. Man, A. Kukulka, S. De Lombaert, Structure-based optimization of arylamides as inhibitors of soluble epoxide hydrolase, J. Med. Chem. 52 (19) (2009) 5880–5895, https://doi.org/10.1021/jm9005302.
[38] C. Cerchia, L. Küfner, O. Werz, A. Lavecchia, Identification of selective 5-LOX and FLAP inhibitors as novel anti-inflammatory agents by ligand-based virtual screening, Eur. J. Med. Chem. 263 (2024), https://doi.org/10.1016/j.ejmech.2023.115932.
[39] P.M. Jordan, J. Gerstmeier, S. Pace, R. Bilancia, Z. Rao, F. Borner, L. Miek, O. Gutierrez-Gutierrez, V. Arakandy, A. Rossi, et al., Staphylococcus aureus-derived alpha-Hemolysin evokes generation of specialized pro-resolving mediators promoting inflammation resolution, Cell Rep. 33 (2) (2020) 108247, https://doi.org/10.1016/j.celrep.2020.108247.
[40] M. Werner, P.M. Jordan, E. Romp, A. Czapka, Z. Rao, C. Kretzer, A. Koeberle, U. Garscha, S. Pace, H.E. Claesson, et al., Targeting biosynthetic networks of the proinflammatory and proresolving lipid metabolome, FASEB J. 33 (5) (2019) 6140–6153, https://doi.org/10.1096/fj.201802509R.
[41] R. Morphy, Z. Rankovic, Designed multiple ligands. An emerging drug discovery paradigm, J. Med. Chem. 48 (21) (2005) 6523–6543, https://doi.org/10.1021/jm058225d.
[42] E. Harder, W. Damm, J. Maple, C. Wu, M. Reboul, J.Y. Xiang, L. Wang, D. Lupyan, M.K. Dahlgren, J.L. Knight, et al., OPLS3: a force field providing broad coverage of drug-like small molecules and proteins, J. Chem. Theory Comput. 12 (1) (2015) 281–296, https://doi.org/10.1021/acs.jctc.5b00864.
[43] K. Roos, C. Wu, W. Damm, M. Reboul, J.M. Stevenson, C. Lu, M.K. Dahlgren, S. Mondal, W. Chen, L. Wang, et al., OPLS3e: extending force field coverage for drug-like small molecules, J. Chem. Theory Comput. 15 (3) (2019) 1863–1874, https://doi.org/10.1021/acs.jctc.8b01026.
[44] W.C. Still, A. Tempczyk, R.C. Hawley, T. Hendrickson, Semianalytical treatment of solvation for molecular mechanics and dynamics, JACS 112 (16) (2002) 6127–6129, https://doi.org/10.1021/ja00172a038.
[45] LigPrep. Schro′dinger Release 2017-1, Schro′dinger, LLC, New York, NY, 2017.
[46] N.C. Gilbert, S.G. Bartlett, M.T. Waight, D.B. Neau, W.E. Boeglin, A.R. Brash, M. E. Newcomer, The structure of human 5-Lipoxygenase, Science 331 (6014) (2011) 217–219, https://doi.org/10.1126/science.1197203.
[47] Protein Preparation Wizard. Schro′dinger Release 2017-1: Schro′dinger Suite 2017-1; Epik, Schro′dinger, LLC; Impact, Schro′dinger, LLC; Prime, Schro′dinger, LLC: New York, NY, 2017.
[48] G. Madhavi Sastry, M. Adzhigirey, T. Day, R. Annabhimoju, W. Sherman, Protein and ligand preparation: parameters, protocols, and influence on virtual screening enrichments, J. Comput. Aided Mol. Des. 27 (3) (2013) 221–234, https://doi.org/10.1007/s10822-013-9644-8.
[49] R.A. Friesner, R.B. Murphy, M.P. Repasky, L.L. Frye, J.R. Greenwood, T.A. Halgren, P.C. Sanschagrin, D.T. Mainz, Extra precision glide: docking and scoring incorporating a model of hydrophobic enclosure for protein−ligand complexes, J. Med. Chem. 49 (21) (2006) 6177–6196, https://doi.org/10.1021/jm051256o.
[50] Glide Schro′dinger. Release 2017-1, Schro′dinger, LLC, New York, NY, 2017.
[51] S. Di Micco, M. Masullo, A.F. Bandak, J.M. Berger, R. Riccio, S. Piacente, G. Bifulco, Garcinol and related polyisoprenylated benzophenones as topoisomerase II inhibitors: biochemical and molecular modeling studies, J. Nat. Prod. 82 (10) (2019) 2768–2779, https://doi.org/10.1021/acs.jnatprod.9b00382.
[52] A. Giordano, F. del Gaudio, C. Johansson, R. Riccio, U. Oppermann, S. Di Micco, Virtual fragment screening identification of a Quinoline-5,8-dicarboxylic acid derivative as a selective JMJD3 inhibitor, ChemMedChem 13 (12) (2018) 1160–1164, https://doi.org/10.1002/cmdc.201800198.
[53] A. Giordano, G. Forte, S. Terracciano, A. Russo, M. Sala, M.C. Scala, C. Johansson, U. Oppermann, R. Riccio, I. Bruno, et al., Identification of the 2-Benzoxazol-2-yl-phenol scaffold as new hit for JMJD3 inhibition, ACS Med. Che. Lett. 10 (4) (2019) 601–605, https://doi.org/10.1021/acsmedchemlett.8b00589.
[54] W. Sherman, H.S. Beard, R. Farid, Use of an induced fit receptor structure in virtual screening, Chem. Biol. Drug Des. 67 (1) (2005) 83–84, https://doi.org/10.1111/j.1747-0285.2005.00327.x.
[55] W. Sherman, T. Day, M.P. Jacobson, R.A. Friesner, R. Farid, Novel procedure for modeling ligand/receptor induced fit effects, J. Med. Chem. 49 (2) (2005) 534–553, https://doi.org/10.1021/jm050540c.
[56] L. Fischer, D. Szellas, O. Rådmark, D. Steinhilber, O. Werz, Phosphorylation- and stimulus-dependent inhibition of cellular 5-lipoxygenase activity by nonredox-type inhibitors, FASEB J. 17 (8) (2003) 1–24, https://doi.org/10.1096/fj.02-0815fje.
[57] A. Koeberle, E. Muñoz, G.B. Appendino, A. Minassi, S. Pace, A. Rossi, C. Weinigel, D. Barz, L. Sautebin, D. Caprioglio, et al., SAR studies on curcumin's pro-inflammatory targets: discovery of prenylated pyrazolocurcuminoids as potent and selective novel inhibitors of 5-lipoxygenase, J. Med. Chem. 57 (13) (2014) 5638–5648, https://doi.org/10.1021/jm500308c. From NLM.
[58] A. Koeberle, U. Siemoneit, U. Bühring, H. Northoff, S. Laufer, W. Albrecht, O. Werz, Licofelone suppresses prostaglandin E2 formation by interference with the inducible microsomal prostaglandin E2 synthase-1, J Pharmacol Exp Ther 326 (3) (2008) 975–982, https://doi.org/10.1124/jpet.108.139444. From NLM.
[59] K. Günther, C. Ehrhardt, O. Werz, P.M. Jordan, Protocol for lipid mediator profiling and phenotyping of human M1- and M2-monocyte-derived macrophages during host-pathogen interactions, STAR Protoc 5 (3) (2024) 103142, https://doi.org/10.1016/j.xpro.2024.103142. From NLM.
[60] P.M. Jordan, K. Günther, V. Nischang, Y. Ning, S. Deinhardt-Emmer, C. Ehrhardt, O. Werz, Influenza A virus selectively elevates prostaglandin E(2) formation in pro-resolving macrophages, iScience 27 (1) (2024) 108775, https://doi.org/10.1016/j.isci.2023.108775. From NLM.
[61] O. Werz, J. Gerstmeier, S. Libreros, X. De la Rosa, M. Werner, P.C. Norris, N. Chiang, C.N. Serhan, Human macrophages differentially produce specific resolvin or leukotriene signals that depend on bacterial pathogenicity, Nat. Commun. 9 (1) (2018) 59, https://doi.org/10.1038/s41467-017-02538-5. From NLM.